Structural Resistance of Earthbag Housing Subject to Horizontal Loading

Student: Chris Croft
Supervisor: Dr Andrew Heath

Department of Architecture and Civil Engineering
The University of Bath
2011

AR40223 MEng dissertation

Abstract

Earthbag housing is a recent development that offers a low cost and low carbon housing solution. Little is known of the structural performance of earthbag housing and this paper seeks to address this by investigating the resistance of earthbag structures to horizontal loading. Walls have been tested by applying loading longitudinally and perpendicular to the length, and comparisons have been made with theoretical models.

The contribution to strength of different variables used in conventional design has been examined. It was found that the addition of cement render provided the greatest improvement both in strength and stiffness and for both directions. For variables other than render, the serviceability limit state was defined as the most critical.

Theoretical models for the in-plane loading showed good correlation with the experiments, although imperfect modelling resulted in erroneous predictions for the failure mode of walls subject to out-of plane loading.

Acknowledgements

Great gratitude is extended to Dr. Andrew Heath for his enthusiastic support and guidance throughout this research project. Dr Michael Patterson also provided the know-how on areas less familiar to the author and this proved highly valuable.

The author would also like to thank the laboratory staff who included Will Bazeley, Neil Price, Brian Purnell, Graham Mott and Sophie Hayward. A fantastic effort was made to achieve a large number of experiments in such a short space of time.

One last thank you is for Ellen. Although not familiar to the world of earthbags before, she has provided great support in producing this contribution.

Table of contents

List of Figures

List of Tables

List of Symbols

A	Contact area between two bags
$A_{cross\ section}$	Area of cross-section
b	Bag width
c	Effective cohesion
$\overline{c}$	Modified effective cohesion
h	Bag height
H	Horizontal load
$H_{failure}$	Horizontal failure load
$H_{F,Bending}$	Horizontal bending failure load
$H_{F,Shear}$	Horizontal shear failure load
I_{render}	Second moment of area of render
I_{xx}	Second moment of area of section
K_a	Active earth pressure (of fill)
l_{crack}	Assumed crack length in render
$l_{cross\ section,bag}$	Length of bag material in cross-section
l_H	Length between top of wall and top lateral load
L	Bag length
M	Applied moment
n	Number of bags above failure plain
N	Applied vertical force
t	Thickness of render
T	Tension force in bag material
w	Earthbag weight
y	Distance to extreme fibres of section
$\bar{y}$	Distance to centroid of area
μ	Coefficient of friction
$\overline{\mu}$	Modified coefficient of friction
σ_{min}	Minimum normal stress
σ_N	Vertical stress
σ_x	Normal stress in the x direction
σ_y	Normal stress in the y direction
σ_B	Stress due to bending
σ_t	Tensile stress
$\sigma_{t,max}$	Maximum tensile stress
$\sigma_{t_{max},render}$	Maximum tensile stress in render
τ_{max}	Maximum shear stress
$\tau_{xy}\ and\ \tau$	Shear stress
φ	Pattern interlocking factor

1 Introduction

Earthbag housing is an intriguing innovation, which is becoming increasingly relevant in a carbon-conscious and still developing world. The ability to construct shelters with the materials available on any site, with the only prerequisites being a supply of lightweight polypropylene bags and several extra hands is a very useful one. It is this simplicity and their inherent sustainability that make earthbags (more commonly referred to as sandbags) a useful building material for use as disaster shelters as well as permanent housing.

Historically militaries have utilised this building method fairly extensively for temporary outposts and for domestic applications such as flood defence retaining walls. In the 20th century their use spread globally and in 1970s Germany, Gernot Minke explored earthbag domes, or flexible rammed earth, for use as low cost, earthquake resistant houses in Guatemala (Minke, 2006). Subsequently an Iranian architect called Nader Khalili working in California has greatly developed their use as permanent and 'modern' houses (Khalili and Vittore, 1998).

Khalili founded Cal-Earth (The California Institute of Earth Art and Architecture) where several prototypes and projects have been undertaken as shown in Figure 1. Through their innovation Cal Earth has brought earthbag housing up to a modern standard, incorporating modern luxuries into the designs (such as electricity and other utilities). Moreover, the geographical setting for these structures is a seismic region and therefore they are at risk to very high loading. They publicise their work through training courses and magazine articles yet uptake of the 'eco-friendly' natural building materials in the western world is still a niche market.

Figure 1 Earthbag Domes at Cal Earth

Earthbag housing is 'low technology' which means it is highly suited to developing economies as well, especially because materials are locally sourced and require minimal processing. It is a technique with high potential in both contexts and research into the material has a universal relevance.

1.1 Earthbag house design and principles

Although there are many styles of earthbag building, they generally adhere to similar design principles to utilise the best of the materials. The flexible form of construction has led to dome forms and non-linear plans which have advantages such as additional strength (hoop stresses) and increased stiffness. For linear walls buttresses have been used to provide lateral support and are recommended to be spaced approximately every 5m (Hunter and Kiffmeyer, 2004).

'Earthbags' is the umbrella term for both the smaller manoeuvrable bags (20-100kg) and the tubing seen in Figure 1 (which comes in rolls of hundreds of meters). The bags or the tubing are filled with earth, laid in place and tamped firm (either by hand or mechanically) to form a hard block, or course. Barbwire is often laid between courses to provide greater control during construction and to link courses so they can act compositely. The houses can also be rendered, which greatly increases the stiffness and durability. Render protects the polypropylene from UV damage and moisture infiltration. Little research has been undertaken to investigate whether the effects of the barbwire in providing a shear link, or the structural interaction between render and bags are significant (see §2.2).

1.2 Advantages and Disadvantages of Earthbag Construction

As mentioned above, the low cost and wide availability of materials are great advantages to using earthbags. Also, the relatively straight-forward construction technique is highly adaptable with no pre determined limits on dimensions or the possibility of annexes. An advantage earthbag structures have over timber shelters is the inherent thermal mass, which provides insulation from extreme external temperatures and dampens high diurnal fluctuations.

In contexts where sustainability is a key design criterion, the most crucial attribute of earthbags is their low embodied energy, which equates to a lower carbon footprint for the housing. Furthermore it has the potential for reuse or recycling of the constituents once the service life of the structure is over. For areas subject to frequent and destructive natural disasters earthbags are thus a sustainable option where re-housing is an issue.

One of the drawbacks of earthbag structures is the high labour demand for tamping down each course of bags (however the skills required are simple and easily taught). Secondly, as with many natural building materials, there is little or no authoritative guidance in the form of building codes or standards to provide a guide on the design or assessment of structures. Finally there may be cultural barriers relating to the image of earthbag houses as suitable modern houses (Daigle, 2008).

One of the many barriers to creating technical guidance is the complex behaviour of the material under load. It does not behave linear-elastically since the bags are deformable, which means you cannot compare it entirely to more popular materials such clay fired masonry (which behaves rigidly).

1.3 Existing codes of practice and previous research

Australia, New Zealand, Spain and Zimbabwe are among the countries which provide national guidance for construction with earthen materials. In general they focus on adobe, pressed earth brick or rammed earth construction and do not take into account the specifics of a bagged form of earthen construction, which could be quite different due to the influence of

soil-bag and bag-bag interaction. There are, however, numerous guidelines and resources available on the internet for small scale projects.

A small body of research has been conducted over the last 10 years investigating earthbags for use in geotechnical structures as well as in housing. The bulk has focused on the strength of the individual bags or stacks, up to 9 bags high, under compressive loading. Previous research is discussed in full in §2.

1.4 Context and aims of research

A typical cross-section of an earthbag dome and the forces it may experience are shown diagrammatically in Figure 2. Walls must resist forces from the roof (incl. self weight, transfer of wind loading and uplift) as well as from direct lateral loading (from the wind, the ground and elsewhere). The loads are either out-of-plane (perpendicular to the wall) or in-plane (along the wall). In conventional design the walls are rendered on both sides and include barbwire and steel reinforcement which will provide additional strength.

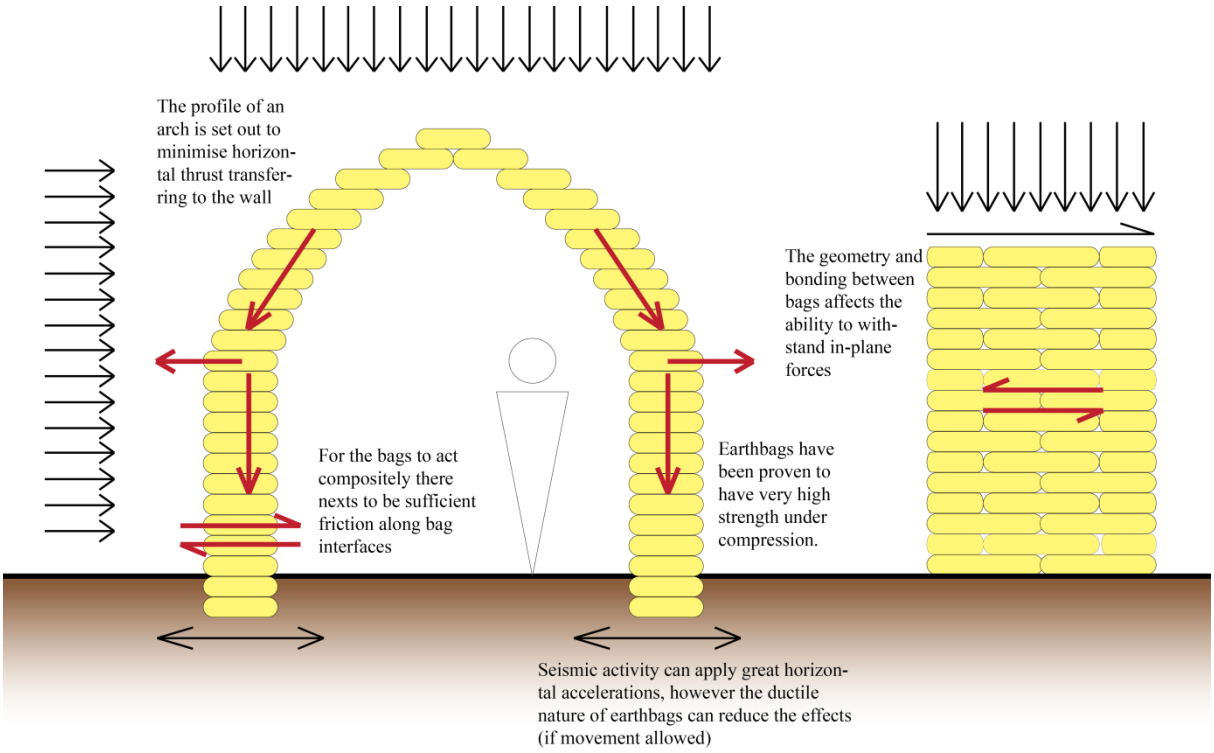

Figure 2 Earthbag dome section (left) and earthbag wall under shear (right)

How do earthbag walls behave under horizontal loading? Do they have adequate strength on their own, or, is barbwire and/or rendering necessary? What is the strength of a wall in terms of ultimate limit and serviceability limit states? What is an appropriate method of analysis for earthbag walls and structures? These are the questions that this research sets out to answer.

2 Literature Review

Earthbag building is a relatively unexplored subject in academic research. A full awareness of previous research projects and studies is important to evaluate previous findings as well as investigate the gaps in current knowledge. A review of applicable literature has been conducted below.

2.1 Earthbag Theory

2.1.1 Compressive strength

Tantono (2007) explored the behaviour of earthbags, by both creating an analytical model and by running numerical simulations using finite element analysis (which was based on continuum theory). It is Tantono's analytical model which provides a basis on which the current theory for compression analysis. Free body diagrams were used to calculate force equilibrium by using of the stress ratio K, to find the horizontal force exerted from the soil on the bag due to vertical loading. Tantono explored modelling the bag with both rectangular ends and semi circular ends (see Figure 3).

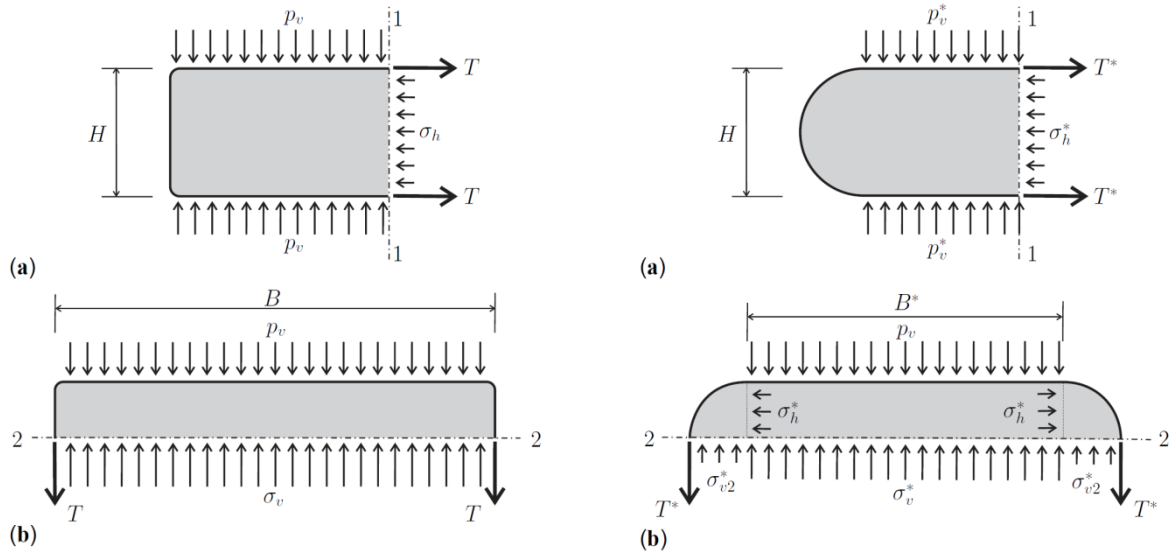

Figure 3 Free body diagrams of rectangular earthbag model (left) and semi-circular model (right) (Tantono, 2007)

By assuming a stress ratio for the soil and knowing the properties of the fill material, the failure load of a bag under compression can then be estimated by equating the tensile capacity of the bag to T shown in the diagram (assuming the bag fails on the top and bottom). However the situation is further complicated by soil-bag interaction and non-uniform stress ratio distributions. The simple equilibrium analysis cannot account for these additional variables so Tantono used finite element analysis to examine the development of stress and deformation.

The compression theory was evaluated by Pelly (2010) and Vadgama (2010) who added to existing theory and produced a simplified analysis assuming plane strain condition. Vadgama (2010) modelled the bags both with rectangular and semi-circular ends. They found that the predicted failure load of the semi-circular model was more accurate, although still an overestimation.

However, a simple prediction (assuming rectangular model), formulated by Pelly (2010) is given by:

$$N = \frac{2T}{K_a h} \cdot Lb \qquad \textbf{(1)}$$

2.1.2 Shear Strength

Vadgama (2010) described the shear strength of earthbags in terms of equilibrium analysis taking into account both the friction between bags and the effect of barbwire between courses. Coulomb friction theory states that the cohesion and coefficient of friction along an interface govern the frictional resistance, regardless of the area over which the normal load is applied. Vadgama (2010) stipulates that the point of a barb will be sufficiently stiff compared to the moment capacity between the point and the strand. Therefore the assumed mode of failure is rotation as a rigid body. However, failure occurs once the bag tears and this was not fully analysed.

The use of barbed wire to resist out of plane shear forces in earthbags was also considered. As shown in Figure 4, the strand of the barbwire would rotate and resist the lateral movement between two bags. The barbwire points in each bag are assumed to tear the bags and fail before the strand yields. This assumption allowed Vadgama (2010) to predict the resisting force due to the translation of the bags. Vadgama (2010) compared this to the compressive force exerted on the translating bag by adjacent bags given a curved wall shape. He concluded that this force was significantly higher than that of the resisting barbwire.

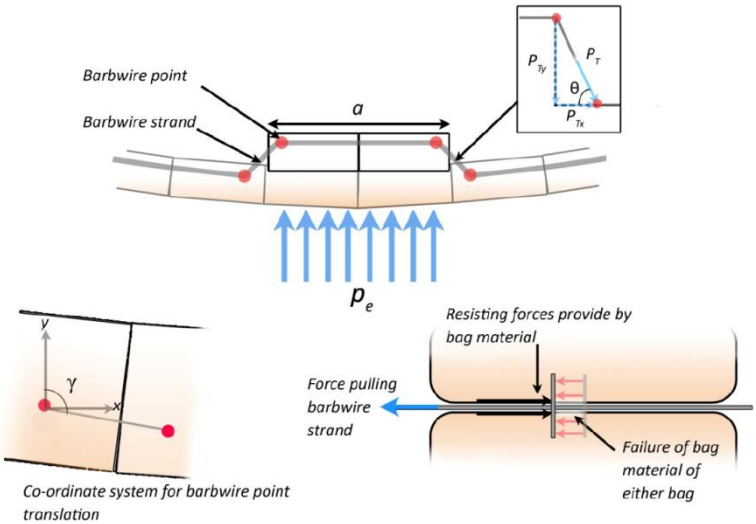

Figure 4 Predicted shear failure mode of earthbags in a dome structure subject to a line load (Vadgama, 2010)

2.2 Earthbag Experiments

2.2.1 Compressive strength

The most tested structural characteristic of earthbags is the compressive strength. Daigle (2008) found that strength decreases with increased stack height and varied according to the fill. Topsoil, sandy soil and crushed granite fill were tested and each proved to have strengths

of 1-3MPa for a stack height of 3. The granite fill bags were tested at 6 and 9 bag heights and strength decrease to ~0.4MPa and ~0.3MPa respectively. Daigle (2008) cited the end restraint affected the strength by providing friction to the bag material which inhibits tensile failure of the bag.

A further set of compression testing was undertaken by Pelly (2010) and Vadgama (2010). They sought to find the limit of the end restraint effects found by once the height to width ratio of a stack becomes greater than 3.0 the effects become minimal. The fill used was fine builder's sand and both ordinary and stabilised fills were tests in polypropylene bags. In terms of strength, Pelly (2010) found that for an 8 bag stack height the non-stabilised stack achieved a strength of 0.97N/mm^2 while the stabilised stack achieved 1.37N/mm^2.

Pelly (2010) and Vadgama (2010) also investigated whether the amount of fill influences the strength. Different amounts of fill were added to 3 bag high stacks however the small stack height led to end restraint effects invalidating the results. More research is needed to gather a better understanding of this variable.

Finally, arch tests were also conducted by Pelly (2010) and Vadgama (2010) as shown, along with the eight bag stack compression test in Figure 5. Stabilised and non-stabilised arches as well as arches with barbwire laid between bags were tested. The main finding was that stabilisation of bags increased the strength by up to 76% compared to non-stabilised arches. Large deflections occurred for both the non-stabilised arch and the arch with barbwire, which exceeded serviceability limits before ultimate limit were reached. This deformability was critical in the arch form and since the stabilised bags were 'hard', the stabilised arches did not fail by sliding and showed greater stiffness. The barbwire was considered to improve ease of construction and post-peak behaviour however it did not improve ultimate strength.

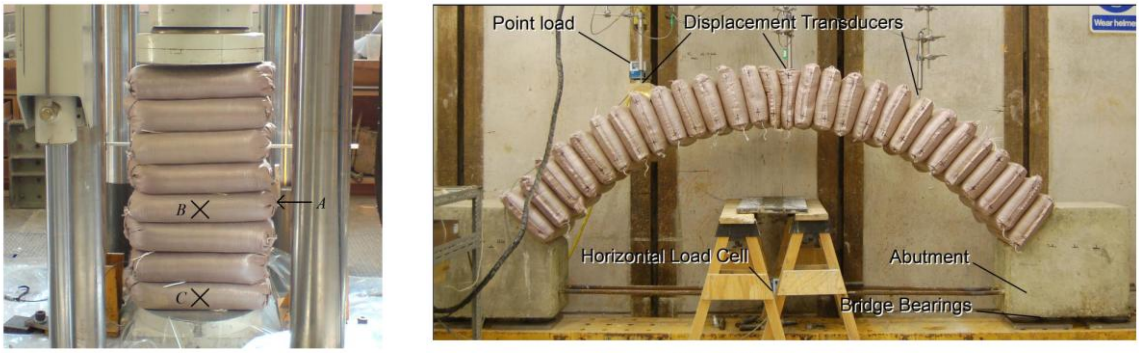

Figure 5 Compression test (left) and arch test (right), Pelly (2010) and Vadgama (2010)

2.2.2 Shear tests

To get an indication of the how earthbags affected the shear properties, shearbox tests were undertaken with one bag placed in each half of the shearbox by Pelly (2010) and Vadgama (2010). A second set of tests was conducted with two strands of barbwire placed between the tamped bags. The test setup and the results are presented in Figure 6. It was found that the barbwire not only provided some adhesion along the bag to bag interface, but it also increased the coefficient of friction. It was thought that horizontal confining stress provided the barbwire with effective resistance and hence an increased coefficient of friction (0.66 compared to 0.43 without barbwire).

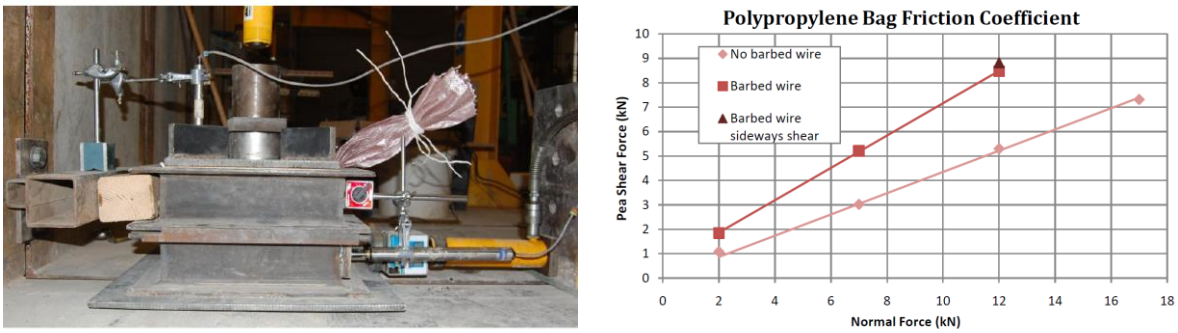

Figure 6 Shearbox tests (left) and accompanying results (right), Pelly (2010)

The barbwire was found to provide 5.5kN/m^2 cohesion along the interface. However, the tests on the bags with no barbwire showed cohesion of 2.3kN/m^2 and therefore the barbwire cohesion was "by no means substantial". Vadgama (2010) went on to state that the effectiveness of the barbwire for shear reinforcement is dependent on several factors:

- Length and orientation of the barbwire point
- Density and strength of soil
- Stiffness of barbwire
- Manor in which the barbwire is laid

Vadgama noted that the barbwire was of benefit in construction since tamping of the bags could generate some shear forces leading to sliding of the newly added course.

Lohani (2006) carried out both compressive and shear (lateral) tests on stacks, in order to understand the overall stability of earthbag structures. The test rig setup for the lateral tests is shown below. A pre-compression force was applied to the upper moving plate in addition to the horizontal load. Polypropylene bags (with a tensile rupture strength of 14.5kN/m) were filled with two types of backfill and weighed 39.0 kg/bag with a water content of 10%. They were stacked in two piles, each four bags high, with each bag compacted with a 6.5 kg hand-operated vibrator for 5–6 minutes. Local vertical deformation transducers (LVDTs) were attached, at varying heights, to the bags.

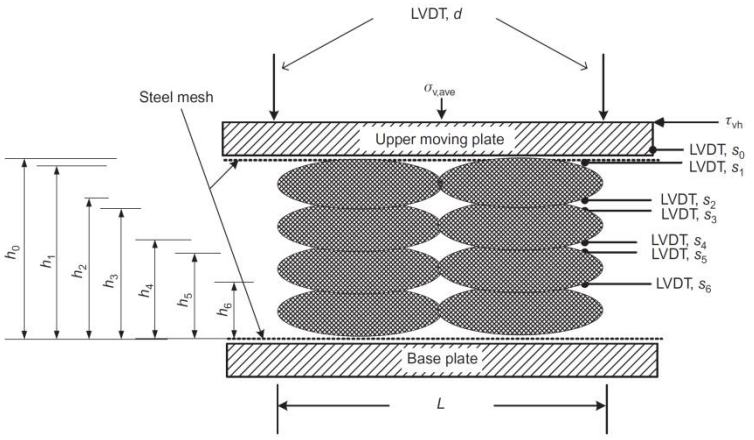

Figure 7 Shear test setup, Lohani (2006)

Four shear tests were carried out on stacks of each backfill type with varying pre-compression forces ($\sigma_{v,ave}$ = 147 , 275 and 400kPa)). Lohani (2006) plotted the strength characteristics deducted from his compression tests to his shear tests and found the failure envelope was much lower and shallower from his shear tests (see Figure 8). This was due to more shear strength in the fill being mobilised in the vertical tests than the lateral tests.

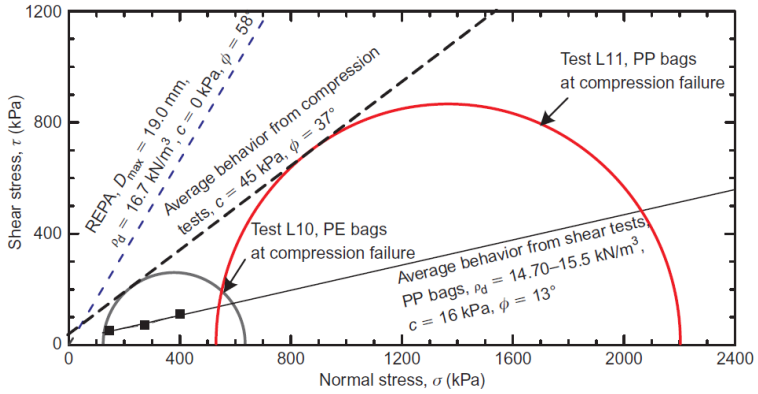

Figure 8 Failure envelope and Mohr's circle plotted by Lohani (2006)

Firstly, in a direct shear box test the increased confinement allows greater complementary shear stresses to develop along the vertical face between the bag and the shear box. However in Lohani's lateral shear tests the bags were not confined and so less complimentary shear stress developed to resist the shearing. Secondly, Lohani (2006) cited "the highly anisotropic nature of the compressive strength of a soil bag" as a reason for decreased realised shear strength. This is because the geometry of the earthbags results in a greater proportion of its strength coming from the horizontal interaction between the vertically adjacent bags than compared to one bag and its fill. These interactions are weaker than the more uniform passive earth pressures seen in vertical compression tests.

2.3 Literature of indirect relevance

When it comes to investigating earthbag walls subject to in-plane horizontal loading, there is no existing research to call upon. Instead the field of masonry subject to horizontal loading has been investigated since compacted earthbags are comparable to masonry blocks.

Turnšek and Čačovič (1971) proposed an elastic, homogeneous and isotropic model for the assessment of masonry walls subject to in-plane loading. They calibrated a theoretical relationship by comparing answers to test results and produced a model for the maximum shear stress given the diagonal tensile strength of masonry and vertical loading.

It was subsequently argued that masonry walls do not perform in a homogeneous and isotropic trend. Mann and Müller (1982) demonstrated that weak head joints (the vertical mortar joints between two blocks) can lead to an alternative distribution of normal and shear stresses on a block with a wall. Ineffective or non existent head joints are unable to provide complimentary shear stresses, which leads to a torsional moment being added to the stress state of the block. This serves to increase the normal stresses on one half of the block and decrease them on the other. This modified state of stress affects the global shear resistance by creating a diagonal stepping failure path of weaker frictional resistance and hence reduces the in-plane strength of the wall.

With great insight Mann and Müller (1982) illustrated this phenomenon by testing a scale model of rubber masonry unit and thick foam mortar with shear and normal loading applied.

It was evident that each block underwent small rotations and hence there was unequal normal stress acting on the blocks within the wall. Following their discovery Mann and Müller (1982) developed a factor to modify the original Mohr-Coulomb frictional properties to better match the lower shear strength of masonry walls.

Bosiljkov et al (2008) have reviewed all the recognised models for the determination of masonry behaviour under in-plane by comparing experimental results with predicted results. This formed part of a wider research project to identify the weaknesses of masonry under seismic loading. It was found that the Turnsěk and Čačovič (1971) model was only accurate to masonry with stiff mortar in both the bed and head joints. On the other hand the Mann and Müller (1982) model was found to be effective for masonry of weak head joints and mortar. It was pointed out that the model can be modified for alternative block geometries, as well as the block tensile and compressive strength.

In the earthbag structures investigated in this paper, no mortar shall be considered and therefore head joints will be unfilled. Furthermore the geometry and strength of earthbags are different to those of masonry. Thus the masonry model given by Mann and Müller (1982) is the most appropriate to apply to earthbag walls.

2.4 Conclusion

In the last eight years a reasonable amount of experimental research has been undertaken on the properties of single earthbags or stacks of earthbags in compression, yet very little testing has been undertaken on the resistance to lateral loading. As a consequence of this, models of how earthbags behave under compression have been developed and experimental results show that the earthbags are strong in compression; they are certainly strong enough to cope with likely vertical loads for houses.

As pointed out in §1.4 above, earthbag housing is subject to forces other than purely vertical forces and therefore an understanding of in-plane and out-of-plane strength is needed. A small number of shear tests have been conducted to investigate the friction between two or more bags and it has been proved that earthbags have a much lower lateral strength than compressive strength. Furthermore it has been recognised for masonry walls that the lateral loading capacity of a wall is not as straightforward as friction between blocks. Calculations assuming the simple friction between masonry blocks overestimate the global wall capacity and this is a possibility for earthbag walls too.

As a starting point in creating a model to determine earthbag strength under lateral loading, the existing masonry wall models will be adopted and evaluated here, given that it is a heavily researched field. The shear strength of masonry walls is a critical aspect of seismic resistance and is therefore considered important to assess the shear strength of earthbag housing.

3 Theory

Earthbag walls are unique in their structural behaviour. Although they are geometrically comparable to masonry or earth brick walls, they are deformable and are confined by a plastic material. This deformable nature can potentially lead to large displacements once the peak strength of the wall is exceeded until ultimate failure. Both serviceability limit states and ultimate states will be observed in the experiments. However, only the linear elastic behaviour is considered in this chapter.

3.1 Behavioural and mechanical assumptions

The theoretical analysis requires certain assumptions to be made in order to establish discernable relationships between two or more physical variables. Up until the linear elastic limit, for the materials and models, the bags are assumed to act rigidly due to their compacted state. In other words, plastic deformations are relatively small and are negligible.

Geometrically, the bags and the courses of bags are examined supposing they are uniform over their length leading to uniform frictional resistance. The materials are also considered to be incompressible which therefore indicates that cross-sections and volume remain constant. Where additional elements such as barbwire, reinforcement and render are included, then composite action between each one and the bags to which they are attached is implied.

Finally, the mechanisms in which loads are applied are assumed to applied loads evenly and results in negligible local deformation. This suggests that loading plates and wall supports are rigid and infinitely stiff.

3.2 Wall design and testing models

To simplify testing and produce more universally applicable results only vertical linear walls have been investigated in this research. Since there are no preceding investigations into the capacity for earthbag walls resisting horizontal loads, then this stipulation provides a useful starting point for further investigations. A design as described in Hunter and Kiffmeyer (2004) has been used to provide a basis for the test model setup, shown in Figure 9.

In the design the loading from the roof is transferred into the wall through timber rafters which bears onto a timber plank. The plank spreads the load over the top course of earthbags and two steel reinforcement bars stake each rafter into the wall. The authors state that the rebar is used to lock the roof to the walls in the event of uplift from wind, however by inspection it is likely to provide additional shear capacity between the top three courses of bags and therefore require a greater number of courses to be mobilised in the event of sliding failure.

Alternative designs either incorporate a concrete ring (or bond) beam, which runs over the top course, or instead of ‘rebar stakes’ above, polypropylene banding is used to tie the timber plate to the top three or four courses. Only the design shown in Figure 9 is considered here which has been modelled by the experiments shown in Figure 10. These tests have been created to test for the shear strength and flexural strength of walls.

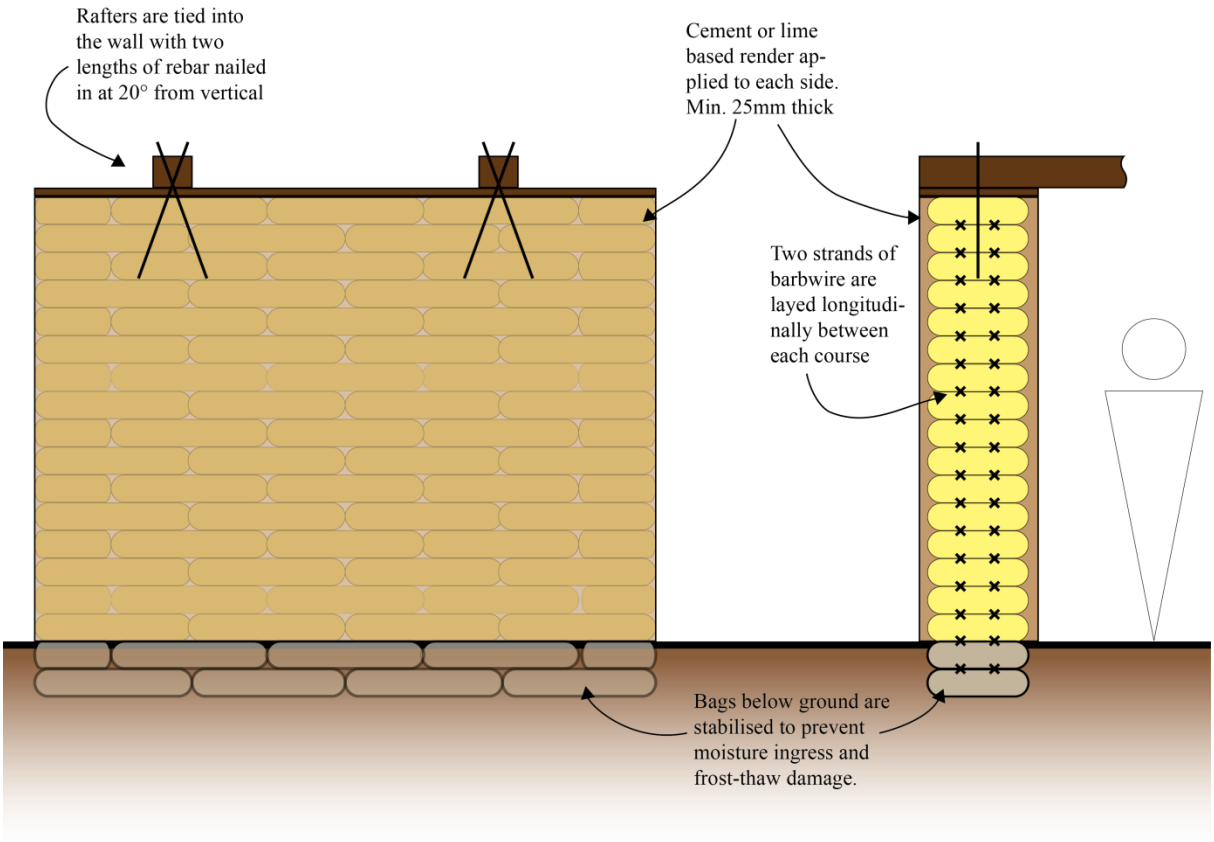

Figure 9 Linear earthbag house wall design, longitudinal section (left) and transverse section (right) (Hunter and Kiffmeyer, 2004)

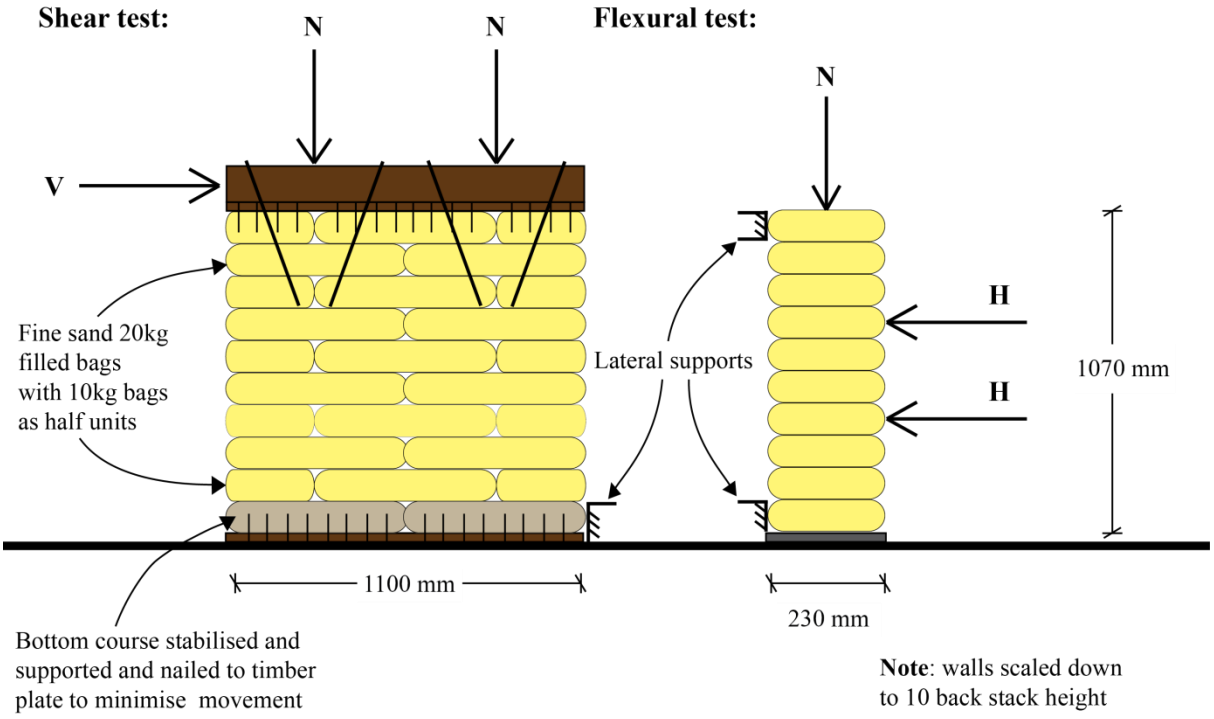

Figure 10 Model walls to be tested in shear (left) and flexure (right) without render or barbwire

Furthermore the characteristics of the model bag are needed to carry out analysis. Measurements were taken for the dimensions and the frictional properties are those found by Vadgama (2010).

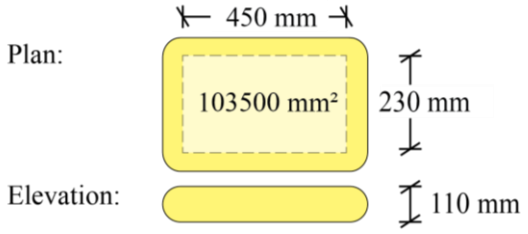

Property	Value
Bag weight (w)	196 N
Contact area (A)	103500 mm^2
Second moment of area (I_{xx})	456 x 10^6 mm^4
Coefficient of friction (μ)	0.43
Cohesion (c)	0
Coefficient of friction w/ barbwire (μ)	0.63
Cohesion w/ barbwire (c)	5.54kN/m^2

Figure 11 Assumed bag dimensions and properties

3.2.1 Shear wall model

The shear wall model has been formed to match the loading conditions and geometrical arrangement seen in the design by Hunter and Kiffmeyer (2004). However a smaller model height has used to allow multiple experiments. The timber rafters have been exchanged for a timber 'spreader beam' of similar cross section to ensure vertical stresses are evenly distributed. Finally, the width of the wall has been limited to two full bags which will produce a lower shear capacity because more failure modes are possible. In this model the shear load is applied via the timber beam to represent lateral loading from the roof only.

The model shown in Figure 10 is the non-rendered 'plain' model without barbwire which will be the benchmark that the further 'rendered' and 'barbwire' models will be compared to. The 'rendered' model is designed as the 'plain' with a cement based render applied to the front and back face. For the 'barbwire' model two strands of barbwire will be laid between each course of bags.

3.2.2 Flexural wall model

A slightly different approach has been used for the flexural test wall in this research. Instead of the roof system being modelled, a base stack of bags is altered with one variable at a time for subsequent tests. The contribution to the flexural strength of cement render, steel reinforcement, barbwire and of stabilising the bags is then investigated. This allows direct comparison between each variable and the results are more generally applicable. The out-of-plane loading has been reduced to two horizontal loads, H, producing a constant bending moment between them.

3.3 Strength of walls in flexure

To determine the strength of the wall in flexure equilibrium of forces is studied. Analysis of the global stress state that the flexural model wall in Figure 10 is under is relatively straightforward. Two mechanisms of failure are possible; either bed-joint sliding or global bending. Buckling has been excluded from this study since it is unlikely to occur for this height of wall. The resistance to each one is then needed to find the lowest and therefore critical strength. To do this the wall has been modelled as a beam and the applied shear and bending stresses determined (Figure 12). Failure occurs once these stresses exceed the accompanying resistance. It is worth pointing out that in each case the applied normal load serves to increase the resistance.

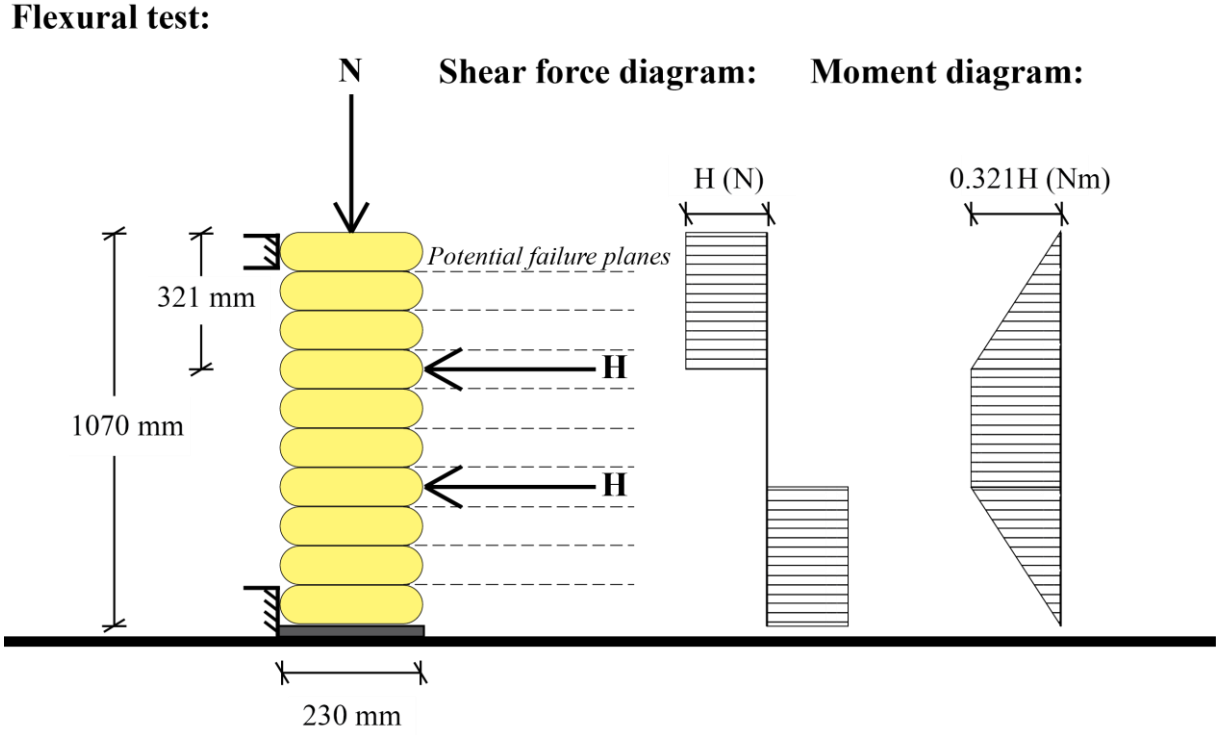

Figure 12 Flexural wall with shear force diagram and bending moment diagram

3.3.1 Failure through sliding

The applied shear force is equal to H, the horizontal load. The plane on which the wall slides will be the plane that has the lowest ratio of shear resistance to shear force. This will be the plane underneath the top bag since the normal force decreases towards the top of the wall (due to reduced self weight). The Coulomb friction equation is used to determine the shear resistance for a given material with an applied normal stress (see, equation (2). The non-dimensional form of the equation for the horizontal failure is given by equation (3). The normal load is increased to account for the self weight of the top course of bags per unit length.

$$\tau = c + \sigma_N \mu \tag{2}$$

$$H_{failure} = Ac + \left(N + \frac{w}{l_H}\right)\mu \tag{3}$$

3.3.2 Failure through bending

To find the capacity of the section in bending, equilibrium analysis is used. As the horizontal forces, H, are applied, a bending moment is induced in the wall. This moment produces tensile stresses on the opposite face and compressive forces on the face to which the loads are applied. Now if we consider the 'plain' model then there is no tensile connection between bags. There are, however, counter-acting compressive stresses due to the self weight of the bags and the normal force. Failure will occur once the tensile stresses, σ_B, from bending are greater than the compressive stresses, σ_N.

$$\sigma_B = \frac{My}{I_{xx}} \quad \textbf{(4)}$$

$$\sigma_N = \frac{N}{A} \quad \textbf{(5)}$$

From equations (4) and (5) the relationship between horizontal failure load, the normal force and the bag properties can be found (where *n* is the number of bags above failure plane, *h* is the bag height):

$$H_{failure} = \frac{I}{Aynh}\left(N + \frac{nw}{l}\right) \quad \textbf{(6)}$$

Given the above formula, it would be logical to assume the critical bending stress is the normal stress on the interface at the same height as the top load. However, if we inspect the deflected shapes given in Figure 13, then at the first surpassing of the normal stress the deflected shape has uneven displacements at the load heights (which would be possible with a single load). In the model examined here the displacements adjacent to the loads must be equal and therefore a greater bending force is needed to displace bags lower down.

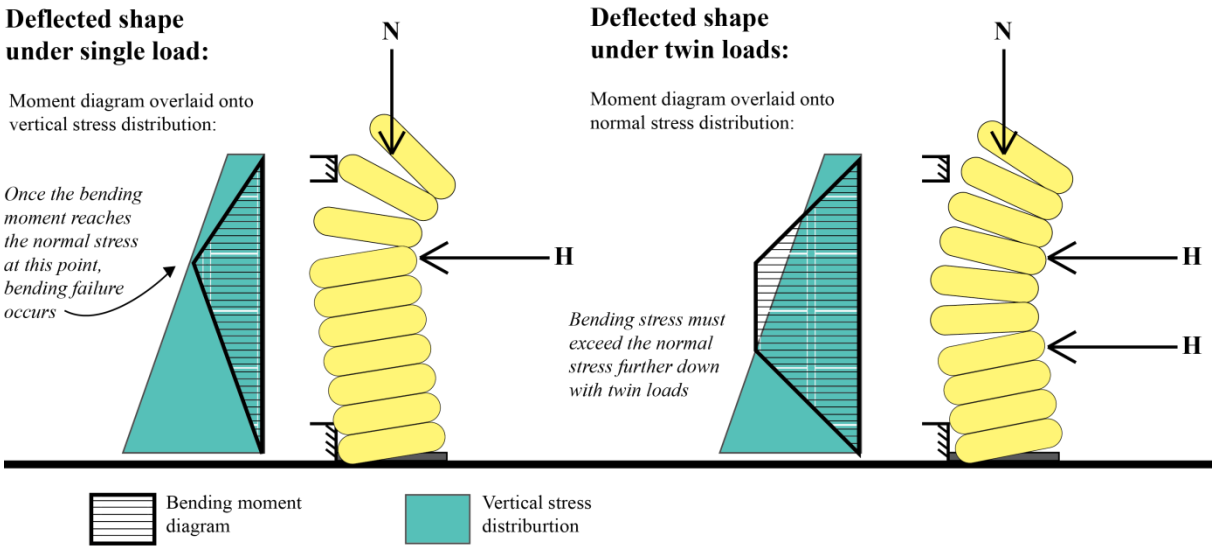

Figure 13 Deflected shape for flexural wall with single (left) and twin (right) applied loads

3.3.3 Predicted failure of the 'plain' model

By substituting in the known values (shown in Figure 11) into equations (3) and (6) we can find the relationship between the normal and horizontal loads at failure for both failure types. These relationships are given in equations (7) and (8).

$$H_{F,Bending} = 0.12(N + n \times w) \quad \textbf{(7)}$$

$$H_{F,Shear} = 0.43(N + w) \quad \textbf{(8)}$$

If we assume *n* is a function of height and a normal load of 1kN, we can predict the failure load for any height of wall of this bag section

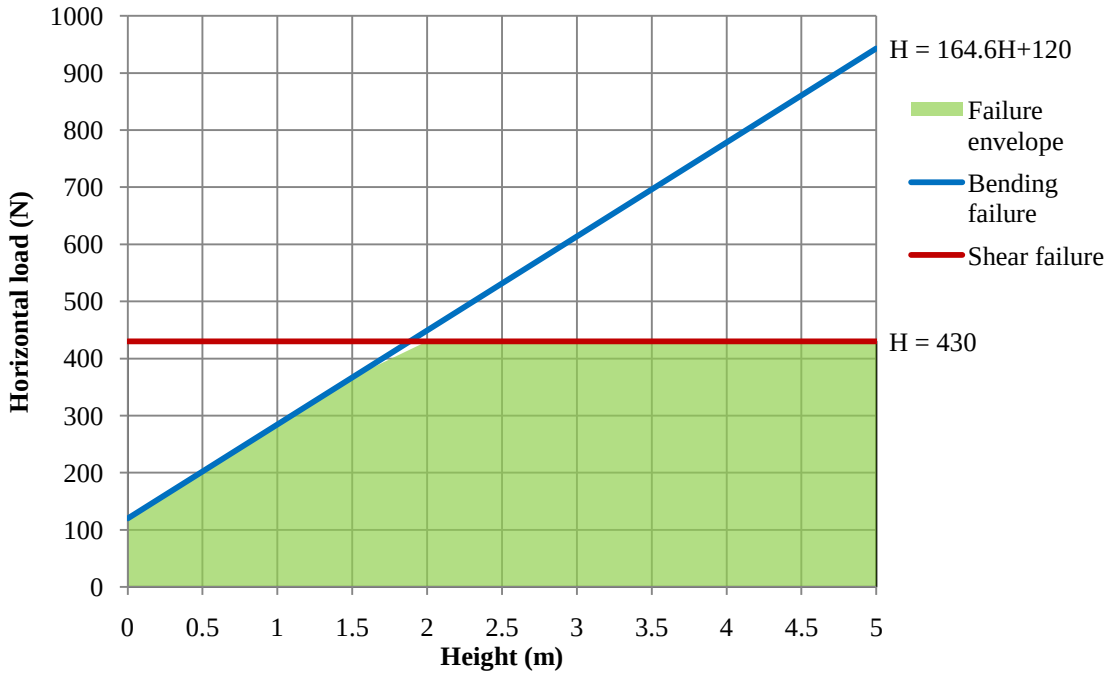

Figure 14 Failure envelope for wall with 1kN normal load per bag

We can see that for walls shorter than 1.8m with a 1kN normal load the failure type will be bending failure. For heights above 1.8m, the wall shear failure governs the strength. In reality buckling would undermine the strength for once the wall becomes slender. The predicted failure type for the wall height tested in this research (1m) is through bending, at a horizontal load (in each jack) of 235.2N (where N=588.6N, the weight of three bags). The shear failure for the same normal load would occur at 337.5N. The failure type for a range of normal loads for a wall of this height is illustrated by Figure 15.

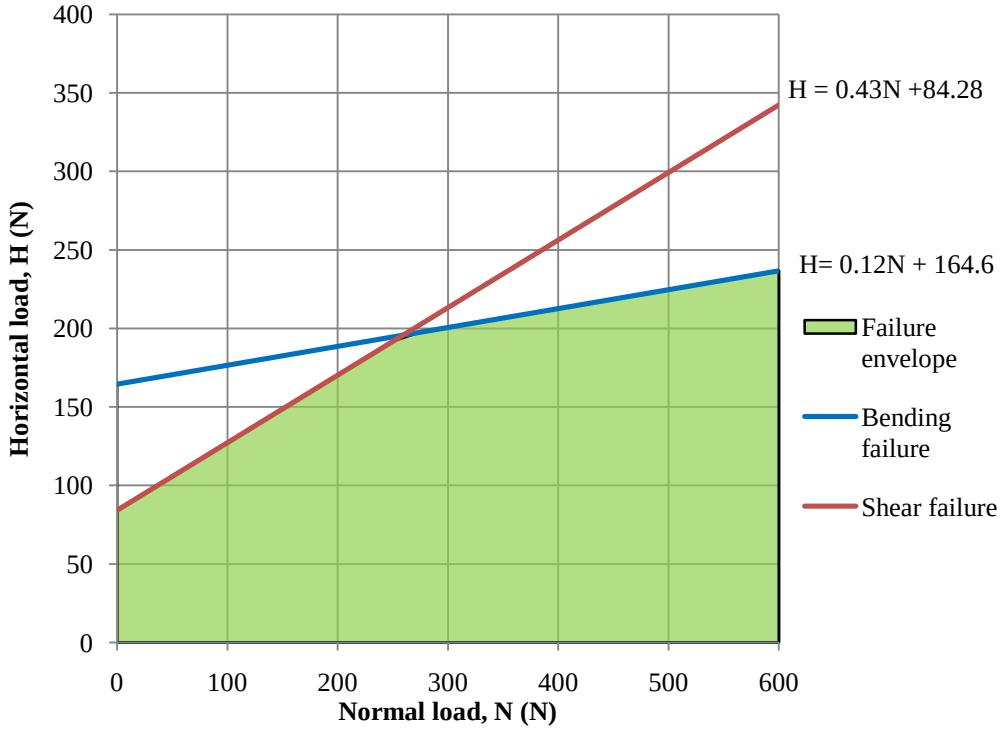

Figure 15 Horizontal load, H, against normal load, N, for a 1m high single bag wall

3.3.4 Effect of reinforcement bar

Although in the design proposed by Hunter and Kiffmeyer (2004) steel reinforcement bar ('rebar') is not inserted through the entire height of the wall, in other such designs it has been. It is believed that this will have a significant impact on the strength and is therefore it is considered an important variable. Now that the strength of the plain model has been calculated, the additional strength provided by inserting rebar is estimated. In the model tested in this research one 10mm steel reinforcement bar is added through the centre of the wall, in line with the neutral axis.

The rebar will add stiffness and strength to the wall as well as acting as a shear link to prevent sliding failure. If we assume a yield strength of 500N/mm^2 then the pre-compression due to the normal load becomes negligible. Independently of the wall, the reinforcement steel, under the same loading conditions, would begin yielding at H=163.7N. If we assume the wall acts compositely then superimposing this strength with the strength of 'plain' wall provides the combined strength of 389.9N.

3.3.5 Effect of barbwire

In the same way that rebar may affect the strength of the walls in flexure, the barbwire that is added between courses may also affect the strength. In the model analysed here two strands of barbwire are added to each bed joint between bags for the barbwire flexural test wall.

Vadgama (2010) showed that barbwire adds a small amount of cohesion (5.54 x 10-3 N/mm2) and increases the coefficient of friction along the bed joints (from 0.43 to 0.67). This increased frictional resistance is not believed to affect the strength however, since the predicted failure for the 'plain' model is through bending. There may be a small amount of additional strength in bending due to the friction force holding the barbs in the bags as the wall begins to rotate. However this is negligible.

For walls greater than 1.8m in height, which is the height from which friction may limit strength (see Figure 14), the increased friction between bags produced by the barbwire is thought to increase strength. No further study has been undertaken because this height of wall is unlikely to be used in earthbag houses.

3.3.6 Effect of stabilisation

Earthbag walls have been stabilised with cement to improve strength and durability in the past (Hunter and Kiffmeyer (2004)). For the analysis carried out here, both the stabilised and non-stabilised bags are assumed to be rigid. This means that the predicted failure load for the stabilised wall is equal to that of the 'plain' wall. In reality it is expected that less deformation of individual bags will occur, which may improve serviceability limit states.

3.3.7 Effect of render

For permanent earthbag structures it is normally the case that they are rendered on each side to extend the service life of the building. In practice often only rule of thumb methods are used in the mixing and application of the render. Therefore it is not believed to be acceptable to rely on any additional strength provided by the render in the design of the earthbag structures, unless tight guidelines are used for the mixing and application. Nevertheless, given that in practice rule of thumb methods are often used, it is still of interest to understand how a rendered earthbag structure will behave under loading. Therefore rendered specimens have been tested in both flexure and shear.

For the flexural test the render (which contains chicken wire) will add tensile capacity to the side of the wall in tension. Parallel axis theorem is used to determine the additional bending resistance by using the equation given below to determine the second moment of area.

$$I_{render} = 2\left(\frac{bt^2}{12} + A\bar{y}^2\right) \quad \textbf{(9)}$$

To provide an estimate the width of render is assumed to be 25mm and the tensile strength equal to 3 N/mm^2. In this scenario the estimate failure load applied is equal to 17.5kN (35kN in total). This is a very high estimated load and will be revised to incorporate the actual results of the tensile strength and thickness, but the render is certainly likely to increase strength dramatically.

3.4 Strength of walls in shear

The behaviour of an earthbag wall subject to in-plane horizontal loading is expected to be significantly different to the out-of-plane behaviour described above because of geometrical differences. Mann and Müller (1982) theorised three types of failure for masonry walls under both shear and normal loading. These are applicable to earthbag walls because up to the linear elastic limit, as mentioned previously, the earthbags are assumed to be rigid. Furthermore, this provides a simple means of primary analysis for earthbag walls.

These three types of failure are as follows:

1. Friction failure of the bed joint
2. Failure due to cracking of masonry units
3. Compressive failure of masonry

These modes will be evaluated for the earthbag shear wall model as shown in Figure 10. Localised failure is not considered due to time limitations.

3.4.1 Friction failure of the bed joint

Conventional Mohr-Coulomb theory suggests that a shear plain will develop along the surface of the least normal load as shown by equation (2). This assumes that the cohesion and coefficient of friction remain constant throughout the wall. Consequently, this method is applicable to masonry walls with filled head joints, which are modelled as homogeneous and isotropic panels (Turnsěk and Čačovič, 1971).

However, the assumption that a masonry wall can act in a homogeneous manor was questioned by Mann and Müller (1982), who considered the bricks and mortar as individual elements which could fail independently of each other. This becomes increasing true if the head joints between units are unfilled or very weak, which is the case for earthbag walls which have unfilled head joints. Without head joints the state of stress that a masonry unit is under in the centre of a wall is modified because complimentary shear stress cannot develop in their absence. Instead, a torsional moment caused by the shear stresses leads to an equal and opposite vertical force couple and therefore an uneven distribution of normal stresses on the block, as shown in Figure 16.

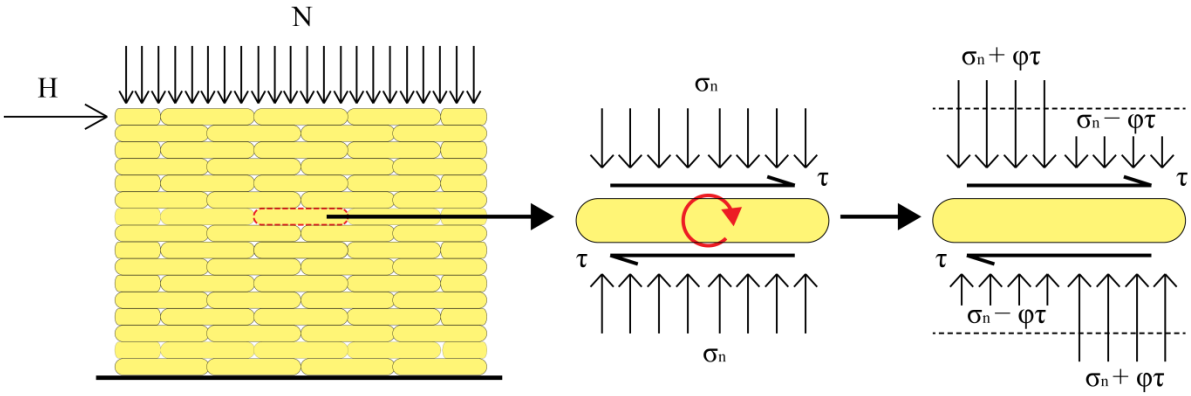

Figure 16 State of stress for masonry unit under shear and normal loading with unfilled head joints

The normal stresses increase and decrease, as the block seeks to rotate by a factor φ, known as the pattern interlocking factor, which is derived from moment equilibrium. This factor is given by:

$$\varphi = \frac{2h}{b} \tag{10}$$

The resulting lower frictional capacity can be expressed in terms of a modified cohesion $\bar{c}$, and coefficient of friction, $\bar{\mu}$.

$$\tau = \bar{c} + \sigma\bar{\mu} \tag{11}$$

The reduced coefficient of friction is derived as follows:

$$\sigma\bar{\mu} = (\sigma - \tau\varphi)\mu = \sigma\mu - \tau\varphi\mu \tag{12}$$

$$\bar{\mu} = \frac{\sigma\mu - \tau\varphi\mu}{\sigma} = \frac{\sigma\mu - \sigma\bar{\mu}\varphi\mu}{\sigma} = \mu - \bar{\mu}\varphi\mu \tag{13}$$

$$\bar{\mu}(1 + \varphi\mu) = \mu \tag{14}$$

$$\bar{\mu} = \frac{\mu}{(1 + \varphi\mu)} \tag{15}$$

A similar derivation is carried out for modified cohesion $\bar{c}$. Although cohesion is irrespective of normal force, it is reduced because the vertical force couple generates counteracting shear stresses and therefore counteracting cohesion. The reduced global frictional capacity in terms of the original frictional properties is given below in equation (16).

$$\tau = \frac{c}{(1 + \varphi\mu)} + \sigma\frac{\mu}{(1 + \varphi\mu)} \tag{16}$$

The areas of lower normal load could lead to a different path of least resistance for the wall to move in sliding because the block halves with lower normal stresses are diagonally opposite

to each other. This is shown diagrammatically by Figure 17, which is an enlarged section of wall in Figure 16.

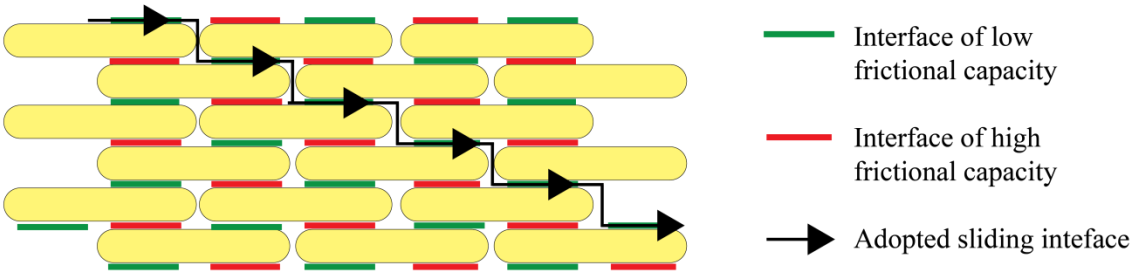

Figure 17 Stepped sliding failure

Whether or not the wall separates diagonally or along one single plane depends on both the block geometry and the distribution of normal stresses across the wall. We can see that as the bag height increases relative to the width, the deviation of the normal stress from the average increases. A simplified approach to determine the average normal stress on a global scale would be to take the stress in centre of the wall.

3.4.2 Failure due to cracking through the earthbags

As the normal load increases, a second type of failure becomes predominant. If we refer back to the actual stress state of a masonry unit in Figure 16, then we find that on every other course, the centre of a unit carries double the shear stress due to the absence of head joints. This heightened shear stress can lead to tensile failure of the unit with a great enough normal force. By examining the stress state of the block on a Mohr's circle we can determine the induced tensile stress force. The generic solution to the maximum stress to Mohr circle is given by:

$$\sigma_{min} = \left(\frac{\sigma_x + \sigma_y}{2}\right) - \sqrt{\left(\frac{\sigma_x - \sigma_y}{2}\right)^2 + \tau_{xy}^2} \tag{17}$$

This equation is adapted to take account for the higher shear stress and the absence of a horizontal stress component in equation (18), which is then rearranged to solve for shear force (equation (19)).

$$\sigma_{min} = \left(\frac{\sigma_n}{2}\right) - \sqrt{\left(\frac{\sigma_n}{2}\right)^2 + 2\tau^2} = \sigma_t \tag{18}$$

$$\tau_{max} = \frac{\sigma_{t,max}}{2}\sqrt{1 + \frac{\sigma_n}{\sigma_{t,max}}} \tag{19}$$

The tensile capacity of an earthbag is comprised of the tensile strength of the bag material divided by the cross sectional area.

$$\sigma_{t,max} = \frac{T l_{cross\ section,bag}}{A_{cross\ section}} \tag{20}$$

3.4.3 Compressive failure of earthbags

The final mode of failure considered here is the compressive failure of earthbags. As we can see from Figure 16, one half the masonry unit is under higher compressive stress because of the torsional moment. The higher compressive stress will lead to a premature compressive failure of the earthbags than if only the average normal and self weight forces were considered. Mann and Müller, 1982, also defined this last parameter:

$$\tau_{max} = \left(\sigma_{c,max} - \sigma_n\right) + \frac{1}{\varphi} \quad \textbf{(21)}$$

3.4.4 Normal stress distribution

The assumed normal stress distribution for the wall will affect the predicted shear resistance. Normal stresses due to normal load alone are distributed evenly across horizontal planes within the wall but those due to the shear force are not. The shear force imposes a moment on the wall which generates a higher normal reaction on the side furthest from the point at which the shear force is applied and reduces the reaction on the side closest to it (in a manner akin to that seen in Figure 16). How exactly the normal loads are adjusted depends on the geometry and the support conditions.

In a comprehensive analysis the normal stress distribution could be calculated with computer software to examine different scenarios. In this circumstance for simplicity since it will return a conservative estimate, the average normal stress in the centre of the wall has been applied. For this model the normal stress is given by:

$$\sigma_n = \frac{2N + 10w}{A_{cross\ section}} \quad \textbf{(22)}$$

3.4.5 Predicted failure of the ‘plain’ model

In the test wall investigated, the reinforcement bar pins the timber beam to the third course of bags. This will ‘join’ the top three course and therefore restrict sliding action between them. Therefore it is predicted that the sliding plane will occur below the third course, which has additional self weight incident upon it and hence requires a greater shear force to slide. As the shear forces increase it is expected there will be some movement of the timber relative to the bags until full passive earth pressure has built up in the bags. The amount of movement will depend on how compacted and confined the fill is. For the plain model the failure envelope has been drawn using the three failure criteria above in Figure 18.

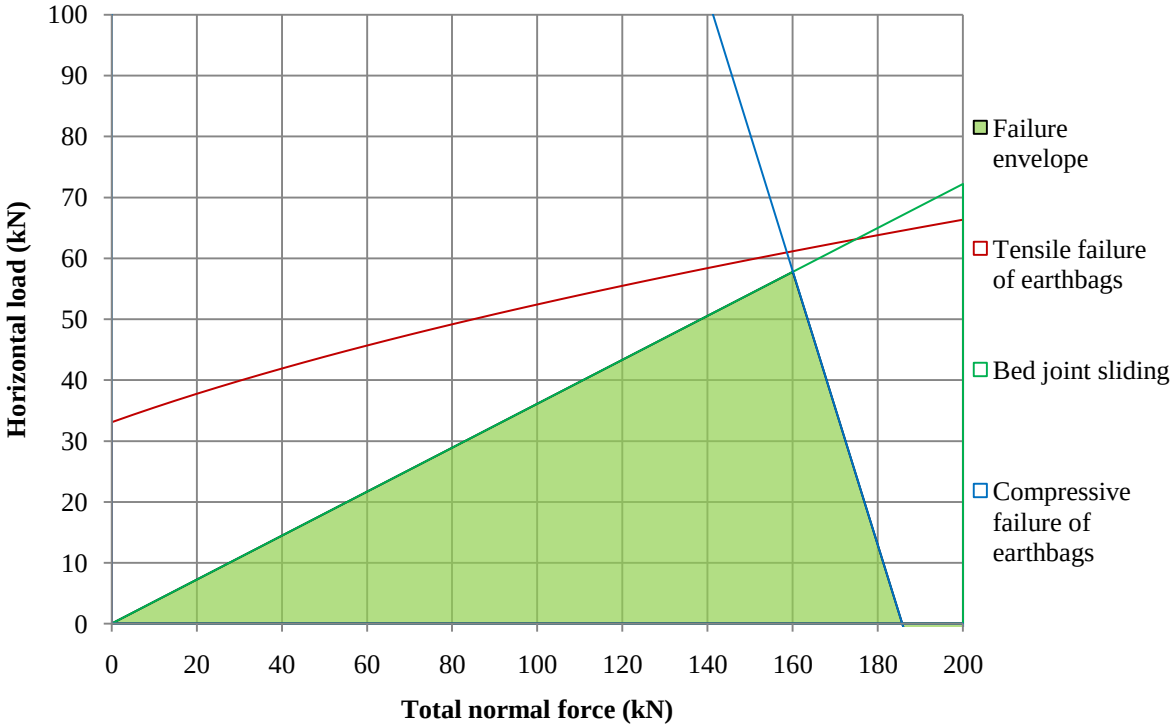

Figure 18 Failure envelope for plain shear wall model

3.4.6 Effect of barbwire

As noted for the flexural test in §3.3.5 the barbwire strands increase cohesion and the coefficient of friction along interfaces. However in the shear wall they may also inhibit diagonal translation of units and therefore alter the failure mechanism. If we imagine a bag moving diagonally over the bag below, then the two strands of barbwire under the top bag must either pull out of one of the moving halves or the strands must yield. This condition is described by Figure 19.

Whether the barbwire strands yield or pull out depends on the amount of friction along both the moving length and the static length. The barbs provide part of this friction and the remainder comes from the bag material and is a function of the normal load. It is difficult to model this friction since both the fixity of the barbs to bags is variable as is the tightness of the barb to the strand.

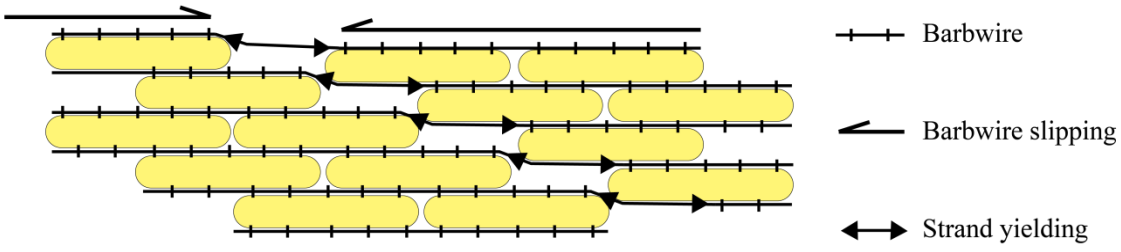

Figure 19 Movement of barbwire in wall under shear

To provide an initial estimate the frictional properties found by Vadgama (2010) have been applied to the horizontal plane under the third course in (23) (units are in mm and N).

$$H_{failure} = 0.0055A_{cross\ section} + 0.63(2N + 6w) \quad \textbf{(23)}$$

3.4.7 Effect of render

The effect of the render is unknown to a large extent. Both faces of render are tied together by steel ties that are looped around the chicken wire mesh before the cement render is cast. These will confine the bags from lateral expansion perpendicular to the direction of the shear force. It is thought that the 'protrusions' of the render between two bags of the same course will key in the 'plates' of render to the bags. These plates will then compositely carry the shear force with the bags.

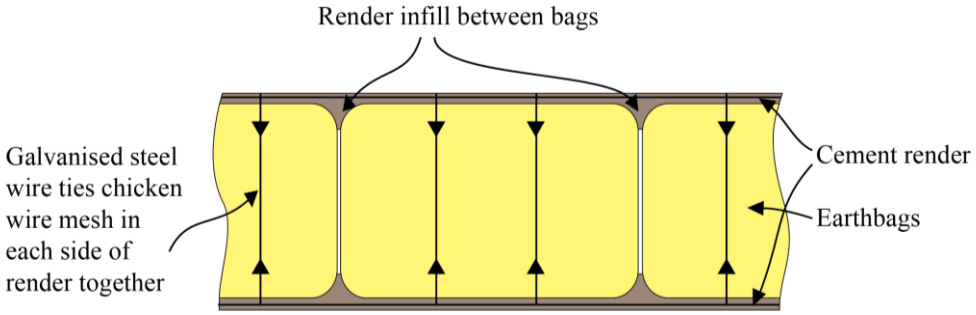

Figure 20 Horizontal section through rendered wall showing render infill and steel ties

As a shear force is incrementally applied it is thought that the bags will compress against the 'protrusions' of render until they shear off or they transfer sufficient tension into the main bodies of render so they split. The resistance due to the render infill is dependent on the number of protrusions in the separating partition and is therefore a function of wall length. The presence of this infill is highly variable and not easily measurable. Furthermore it is assumed that tensile failure is critical since the tensile strength of render is significantly lower than the shear strength. Thus only tensile cracking is investigated here.

Tensile cracking is a function of both the wall length and earthbag geometry. The crack is assumed to occur linearly at angle of 26.3˚ due to the earthbag geometry and the corresponding failure load is given by:

$$H_{failure} = 2\frac{l_{crack} \times \sigma_{T_{max},render} \times t}{\sin(26.3°)} \quad \textbf{(24)}$$

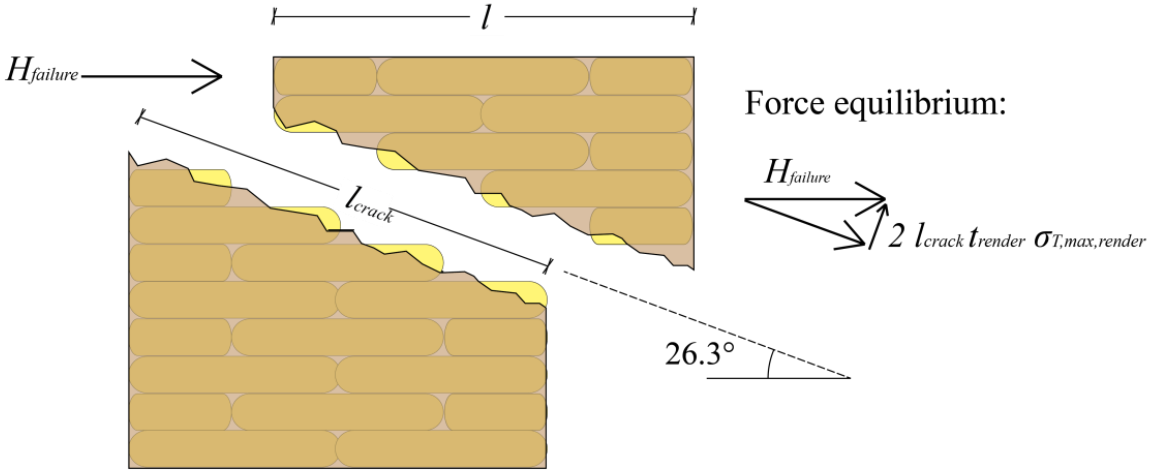

Figure 21 Assumed path for crack in render (left) and force equilibrium (right)

4 Laboratory Testing

Outlined in this chapter are the laboratory experiments that were conducted as part of this investigation. This research succeeds two previous undergraduates' dissertations by Pelly (2010) and Vadgama (2010) which were prompted by a project proposal from a local architecture practice. The dissertations were concerned with a structural and material investigation into the use of earthbag housing in Namibia. Due to this research precedence, the experiments in this report seek to build on their findings. Where applicable, some results from their research have been used in this report rather than conduct repeat experiments.

4.1 Materials

An understanding of the properties of each constituent within earthbag walling systems is needed to interpret results of tests of whole wall sections.

4.1.1 Fill material

The first material to be tested is the fill material. Vadgama (2010) undertook several experiments to determine the properties of the soil and the fill material has been sourced from the same supplies for the tests in this investigation. A sieve analysis was a carried out on the 'fine builder's sand' according to BS 1377 Part II 1990. This sand was the only fill material used in the wall tests.

4.1.2 Bag tensile test

It is the tensile capacity of the bag material that provides the confinement to the fill and it proved to be the limiting factor for an earthbag's strength in compression tests. For the experiments outlined in this research, the tensile capacity of the bag material is a factor of the earthbag wall shear strength at high normal loads.

Strips of 100 gsm polypropylene bag material 50mm wide were clamped with grips into a Dartec 10T loading machine with a pressure of 3000 psi (20.7 MPa). The orientation of samples was such that the longitudinal fibres were parallel to the load and transverse fibres were perpendicular. The tensile load was applied across the whole width at a rate of 6mm per minute for each sample.

4.1.3 Bag tearing tests

A simple bag tearing test was designed to replicate the tearing of bag material by a barb of barbwire or steel reinforcement. Three samples, each 50mm wide, where pinned with nails to small wooden plates, which were then held by clamps in a load testing machine. A tensile force was induced on the bag material until the nails caused a tearing displacement. The amount of material behind the nail (in the direction of the load) was varied. The load increased until the nail or wood began failing at a rate of displacement of 3mm per minute.

4.1.4 Barbwire tensile tests

In the interaction between barbwire and bags it could also be the yield strength of the wire that is the limiting aspect. Three 360mm lengths were stretched longitudinally until they reached yielding point by inducing a constant displacement of 3mm.

4.1.5 Render tests

Flexural tests to BS EN 12390-5:2009 and compression tests to BS EN 12390-3:2009 were carried out on prism samples of render (without chicken wire) that were taken from the render

mixed for the flexural and shear wall tests. The tests were carried out within 24hrs of the full scale tests so the render strengths were equivalent to that experienced in the rendered flexural wall and shear wall tests. The flexural test is an accepted method of finding the tensile strength of the concrete sample.

The displacement was increased at a rate of 2mm per minute while the displacement and load were recorded once per second. The mix for render was of ratio 1:2:2, cement to fine sand to coarse sand. Before the render cured the average thickness was measured.

4.1.6 Rebar tests

In a similar vein to the render tests the solitary strength and behaviour of the steel reinforcement bar provides a useful comparison to the full tests. Sections of bar, 10mm in diameter, were axially stretched, while the displacement and load were recorded. Throughout the full scale tests, 10mm rebar was used. A constant rate of displacement of 1mm per minute to one end of the 150mm samples.

4.2 Wall tests

For the full scale tests the same construction methodology was repeated for each wall. Bags were filled with 20kg of builder's sand then the open end was tied and the flap folded underneath the bag. The bags were placed horizontally on the floor were then tamped with a 13 kg tamper until they became firm.

In the case of stabilised bags being used then 5% cement was added by weight but the total weight of 20kg was kept. No water was added since the sand already had a small moisture content and the bags were left to cure for 7 days. No stabilised or damaged bags were reused. However, the bags from the plain model were loosened after tests and then re-tamped for use again.

4.2.1 Flexural tests

A series of flexural (or bending) tests were carried out on different specimens of wall. The setup is shown diagrammatically in Figure 22 below. Five variations of wall were put under four point bending (producing a constant moment between applied loads). The walls were built 10 bags high and one bag wide and were tested across their minor axis. From here on the individual bags are referred to as numbers 1 to 10, with bag 1 being the top bag adjacent to top support (4^{th} bag down in Figure 22) and bag 10 being the bottom bag.

Six transducers were placed on bags as demonstrated in Figure 22, each with a sensitivity of $1/1000^{th}$ mm and a maximum travel of 100mm. Hydraulic jacks where operated using hand pumps to apply loads to bags 4 and 7. Load cells were attached between the jacks and timber beams, which spread the loads across the width of the bags.

The wall was supported at the top and bottom with the bottom bag resting on a steel plate. Teflon strips were placed between each support and the bags, and between the timber spreader beams and the bags to provide a less frictional interface. To achieve specified normal load simply, additional bags were added onto the top bag. For the increased normal load tests, a normal load of 588N (3 bags) was added.

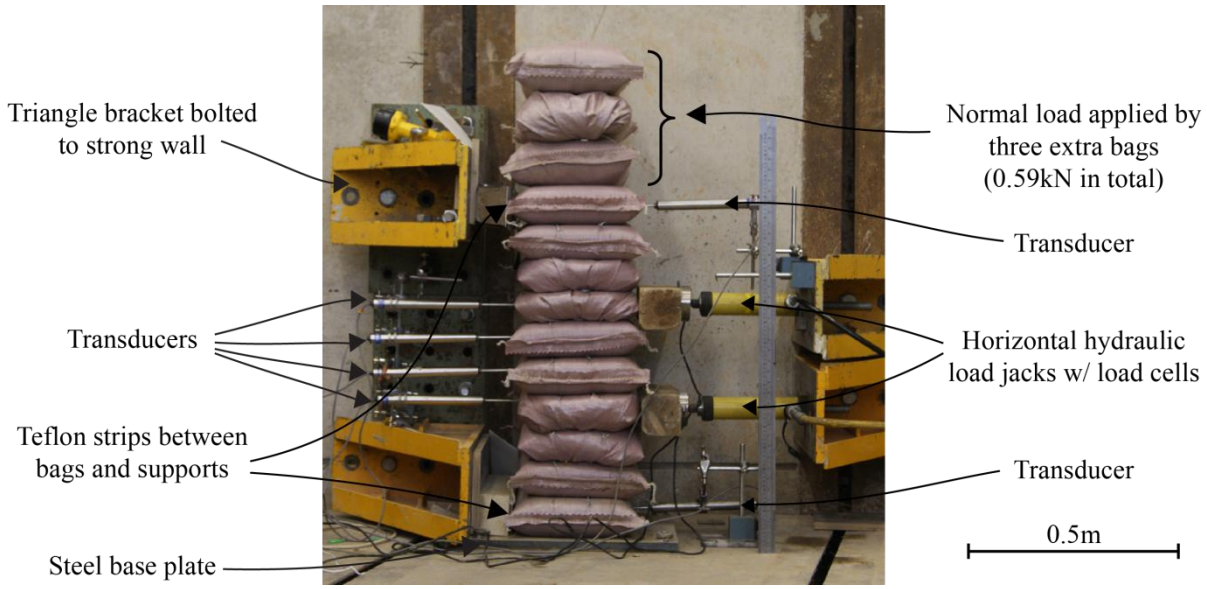

Figure 22 Flexural test setup

A variety of samples were tested and are listed here:

- 10 bag stack with 0 normal load (‘Plain A’)
- 10 bag stack with 196N normal load (‘Plain B’)
- 10 bag stack of stabilised bags with 196N normal load (‘Stabilised’)
- 10 bag stack with two strands of barbwire with 196N normal load (‘Barbwire’)
- 10 bag stack with a 10mm rebar inserted the full height with 196N normal load (‘Reinforced’)
- 10 bag stack rendered both sides with cement render with 196N normal load (‘Rendered’)

4.2.2 Shear tests

The second major set of tests was a set of longitudinal shear tests, which are comparable to racking tests undertaken for different wall panels. The sample walls were constructed 10 bags high and 2 bags long, with a running masonry bond as shown in Figure 23. A timber beam measuring 100 x 100mm was fixed onto a 25mm timber plate that was nailed into the top course of bags to distribute the load evenly. Four sharpened 300mm lengths of rebar were then inserted through the timber plate at 20˚ from the vertical.

Two equal normal loads were applied to the spreader beam by two hydraulic jacks that were attached to one hand pump. Before testing commenced the vertical jacks were locked and effectively became fixed displacements. The lateral load was applied by another hydraulic jack to one end of the timber beam while the wall was supported in the opposite corner by an upright steel section and supporting steel blocks. To ensure even lateral support for the opposite corner, dental plaster was applied between the supported bag and the steel block. Additionally, the bottom course of bags was attached to a 25mm timber board with twelve 60mm steel nails to limit their movement.

Transducers where placed on key bags on each end of the wall and were held in place by hand clamps. 10t Load cells were attached to the hydraulic load jacks and fed into computer along with the transducers’ outputs. Steel rods where inserted into the remaining end bags and

several internal bags where marked with tape to enable photogrammetry to be carried out afterwards to assess displacements.

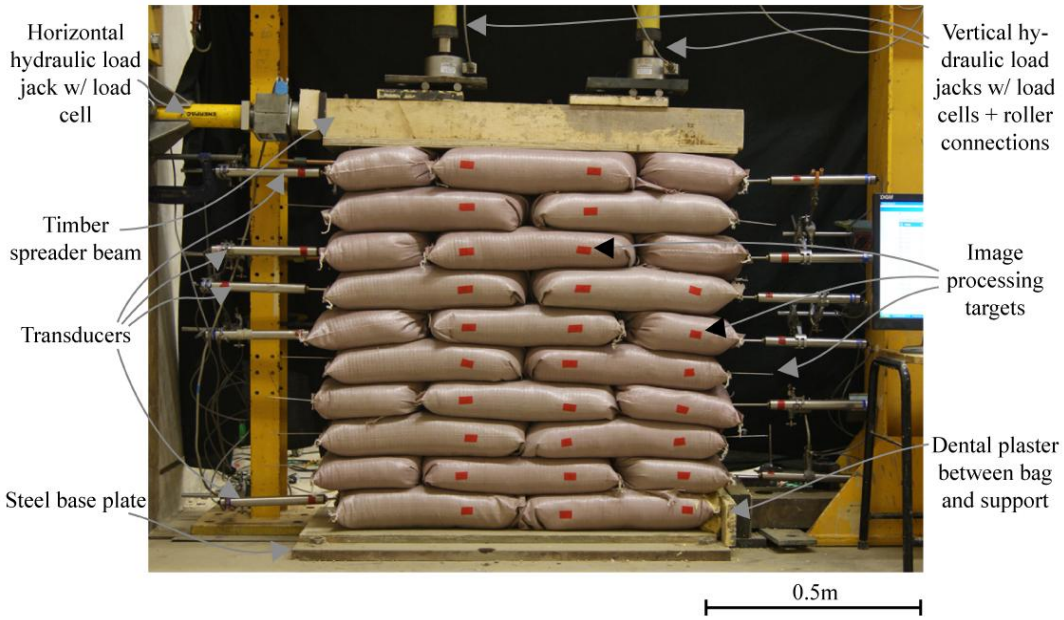

Figure 23 Shear test setup

The following types of shear wall experiments were carried out:

- Plain wall with 0.5kN initial normal load (1kN in total)
- Plain wall with 5kN initial normal load (10kN in total)
- Plain wall with 10kN initial normal load (20kN in total)
- Plain wall with 17kN initial normal load (34kN in total)
- Wall with barbwire between courses with 2 load cycles of 0.5kN initial normal load (1kN in total)
- Rendered wall with 3 cycles with variable normal load (up to 38kN in total)

The photogrammetric analysis was carried out using MATLAB® computer software in conjunction with a unique program written to identify the markers placed on the bags as labelled above. The software reads all input images and plots points of the markers from subsequent images onto the first image to produce a path of movement for each marker.

It was not possible to monitor internal bags for the rendered wall. Instead, DEMEC strain gauges were used to monitor strains within the render. The conical locating points were placed so that three angles were checked in the centre of each face of the wall; one vertical, one at +45˚ and one at one at -45˚.

5 Results & Analysis

In this chapter the results from the laboratory experiments are presented and analysed. To begin with the material component testing results are examined and where appropriate, contrasted to results from previous experiments outlined in §2.2. Following that, the results from the model testing are displayed and investigated in relation to the theoretical predictions made in Chapter 2.

5.1 Materials

5.1.1 Fill material

The sieve analysis carried out confirmed that the fine builder's sand used was approximate to that used by Pelly (2010) and Vadgama (2010). The fill was described as medium grained, of loose – medium compaction, clean and yellow. The particle size distribution is shown in Figure 43 in Appendix A. For the purposes of the following experiments, additional properties of the fill material found by Pelly (2010) and Vadgama (2010) are used.

5.1.2 Bag tensile test

The results from the tensile test of the polypropylene bag material are displayed in Table 1. It was observed that as the samples elongated, contraction of the longitudinal fibres occurred in the mid-point between grips. Peak tensile strength occurred before the fibres on the periphery began snapping until complete failure. The average peak strength observed 12.46N/mm occurred at an average strain of 21.83%. There was a very close correlation between specimens for both stress and strain, yet they are significantly lower than those found by Pelly (2010).

Table 1 Bag tensile test results

Sample	Initial length (mm)	Initial width (mm)	Peak load (N)	Tensile strength (N/mm)	Strain at peak load (%)	Strain at failure (%)
Bag tensile 1	300	50	613.3	12.27	11.33	20.14
Bag tensile 2	297	50	632.0	12.64	10.07	(Failure not reached)
Bag tensile 3	301	50	623.2	12.46	11.21	23.52
Average	-	-	622.9	12.46	10.87	21.83

5.1.3 Bag tearing tests

Tests were carried out with two different lengths of bag material behind the nail (25mm and 50mm). It was noticed that as the transverse fibres adjacent to the nail began elongating, the nail came in contact with more transverse fibres and therefore resistance increased. Initially, rather than yielding, the transverse fibres were seen to slide across the longitudinal fibres to accommodate the movement of the nails. This means that the friction between the transverse and longitudinal fibres was a contributing factor to the strength and so wider strips would have a higher strength.

For the specimen with 25mm of cover, a peak load of 31.18N was reached, whereas the specimen with 50mm of cover reached 139.11N. At approximately 122N yielding of the closest transverse fibres became apparent for the sample with greater cover. It can be argued

both the width and cover to the nail determine the tearing strength. The results from the bag tearing tests are in Table 2.

Table 2 Bag tearing test results

Sample	Initial cover (mm)	Initial width (mm)	Peak load (N)	Tear length at peak load (mm)
Nail 25	25	50	31.18	8.30
Nail 50	50	50	139.11	32.55

Both the tearing and tensile strength of the bag material affect the strength of a wall in shear. The tearing strength determines how much shear load can be transferred to the barbwire, while at high normal loads, the tensile strength of the bag material limits strength of the wall as explained in §3.4.3. From these results we can see there is a large difference between the tensile strength of the bag material and its tearing strength. For both tests 50mm wide samples were used. However at a load of 50N the elongation in the tearing tests was 5x that of the tensile tests, showing that excessive strains are likely at low normal loads where sliding failure is predominant. These tests do not account for the contribution of the fill material which will reduce the strains seen in the wall tests.

As mentioned above, the tearing strength is a function of the length of cover to the nail. By way of comparison, the tearing strength has been projected for longer strips (with more cover) in Figure 24 along with the tensile and tearing results.

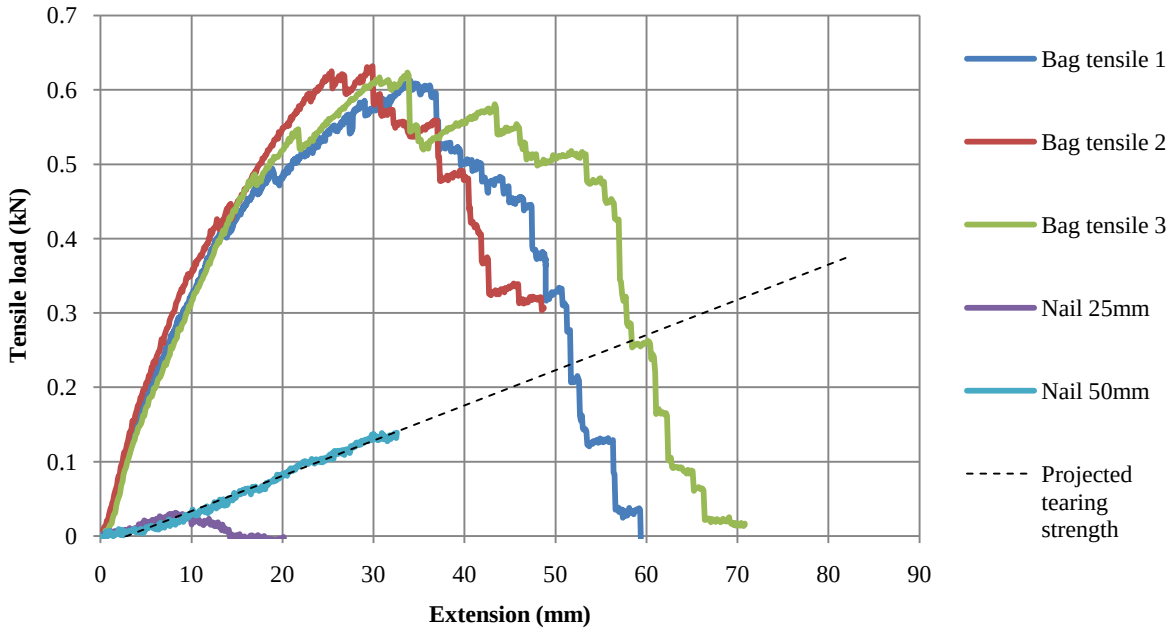

Figure 24 Tensile load vs. extension for bag material tensile and tearing tests

5.1.4 Barbwire tensile tests

It is useful to compare the tearing strength of the bag material with the yield strength of the barbwire to identify the weakness in the connection between the barbwire and the earthbags under friction. The average peak strength was 3.49kN at a strain of 3.05%, with all three

samples strain-hardening beyond the linear elastic range. Table 3 shows a summary of the tests, while the results are plotted in full in Appendix B.

Table 3 Barbwire tensile test results

Sample	Initial length (mm)	Peak load (N)	Strain at peak load (%)	Strain at failure (%)	Young's Modulus (kN/mm^2)
Barbwire 1	364	3673	3.29	4.10	100.45
Barbwire 2	362	3430	3.19	4.06	70.11
Barbwire 3	365	3353	2.67	3.21	78.99
Average	364	3485	3.05	3.79	83.18

As expected the barbwire is far stiffer and stronger than the bag material tearing strength. However, for a wall under a shear load where there is potential for sliding across the bed joint, then this tearing strength is contained in each barb. So if we assume a bag tearing strength of 0.14kN (at an extension of 32.6mm) then we can calculate that the barbwire would need approximately 23 barbs inserted into the bags before the yield strength of the barbwire is approached for a wall in shear. If we assume that each barb is attached to the bag above and bag below then a wall length of approximately 2m contains enough barbs to anchor the wire with enough force that the wire begin to yield. It is therefore unlikely that the barbwire will yield in the tests model examined here, which is only 1m long, but should be considered for longer walls.

5.1.5 Render tests

The compression and tensile tests were carried out on the render that was applied to the flexural model and shear model and the results are tabulated below (Appendix C contains results in full). A modulus of elasticity has been calculated for each render based on the strain during the axial compression tests.

Table 4 Render test results and measurements

Sample (average)	Average thickness (mm)	Minimum thickness (mm)	Compressive strength (N)	Tensile strength (N/mm)	Young's modulus (N/mm^2)
Flexural wall	33.4	14.2	10.13	3.38	1502.5
Shear wall	35.7	16.4	10.89	3.23	1872.7

It is important to remember that the thickness of the render is highly variable due to the curved geometry of the earthbags. The render is thinnest adjacent to the mid-height of the bags (where the bulge is greatest). We can see that at these points the render is less than half as thick as the average and is therefore less than half as strong under tension and compression.

5.1.6 Rebar tests

The average yield stress of the steel reinforcement was $511.8N/mm^2$ while the average yield strain was 0.231%. The full results from the rebar axial tests are displayed in Appendix D and are discussed in §5.3 and §5.5.

5.2 Flexural test results

The results from all of the flexural wall tests are plotted in Figure 25. As expected the strength of the rendered wall was far in excess of the other samples, reaching a peak load approximately nine times that of the rest. The second strongest was the reinforced wall, which initially showed similar behaviour to the others but increasing strength post 'elastic' limit. Of the remaining walls, the barbwire model proved to have a higher ultimate capacity than the plain model or stabilised model.

It terms of stiffness, the rendered wall was considerably stiffer than the others, deforming recoverably until around 5.5kN total horizontal load. This is again in the region of nine times that of the other types tested. Apart from the rendered wall, the stabilised model was the stiffest, followed by the reinforced model, then the plain model. The barbwire model displayed the lowest stiffness yet it did not decrease after the deflection exceeded the elastic limit.

Table 5 summarises the results and on page 32 Figure 26 shows an enlarged view of the elastic and transitional behaviour. All models sustained large displacements beyond peak strength which in the case of the plain, stabilised and rendered models led to the walls bearing onto unintended supports which prematurely halted those experiments. The peak strength was achieved in all cases except that of the reinforced wall, which displayed increasing stiffness in the plastic deflection range. The results have been clipped to show only the true loads attained and normalised against support displacements.

By way of comparison a serviceability deflection equal to span / 250 has been used to gauge serviceability limit strength. Furthermore an equivalent UDL of 2kN/mm^2 (which produces the same maximum moment as twin loads of 0.4kN) has been set against displacement to identify the deflection for each model at this benchmark.

Table 5 Summary of flexural test results

Wall model	Peak load (kN)	Deflection @ 2kN/m^2 UDL equivalent (mm)	Load @ span / 250 serviceability limit (kN)	Failure type	Bending stiffness (kNm^2)
Plain A	0.46	-	0.43	Sliding	-
Plain B	0.88	1.83	0.85	Sliding and bending	7.35
Barbwire	1.40	3.76	0.86	Bending	3.50
Reinforced	1.52	1.22	0.99	Bending	10.84
Stabilised	0.92	0.61	0.87	Sliding	-
Rendered	7.32	0.05	6.01	Bending	59.81

5.2.1 'Plain' model behaviour

Two tests were conducted on the plain model; 'Plain A' was conducted with no applied normal loads and 'Plain B' with 588.6N normal load (as with the other tests). When the horizontal load was applied to 'Plain A' the wall rotated about the bottom bag and a single sliding interface was created under the top support (between bag 1 and bag 2). Very little relative movement occurred between adjacent bags in the rotating body and it was clearly visible that shear failure had occurred.

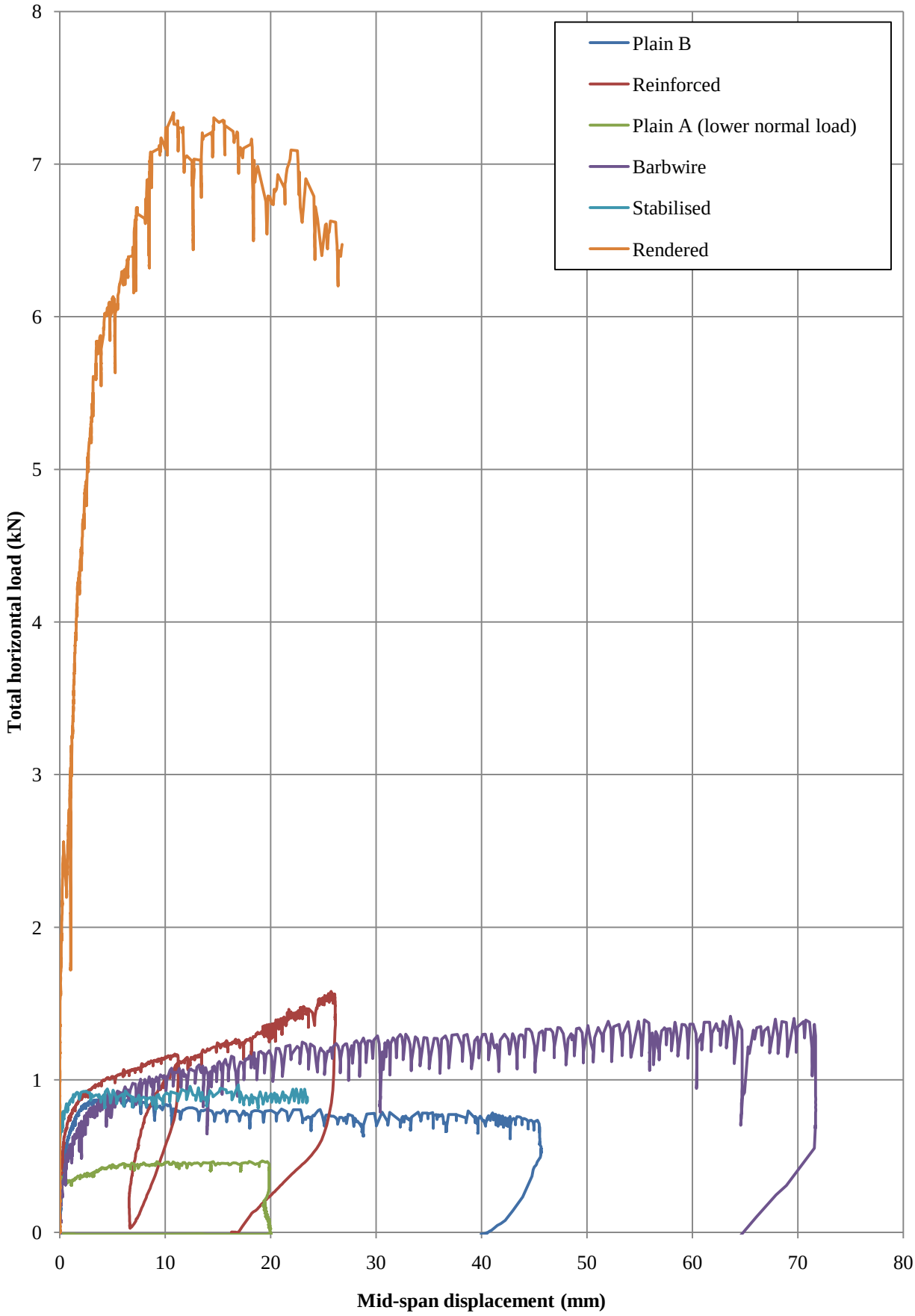

Figure 25 Horizontal load vs. mid-span displacement for flexural wall tests

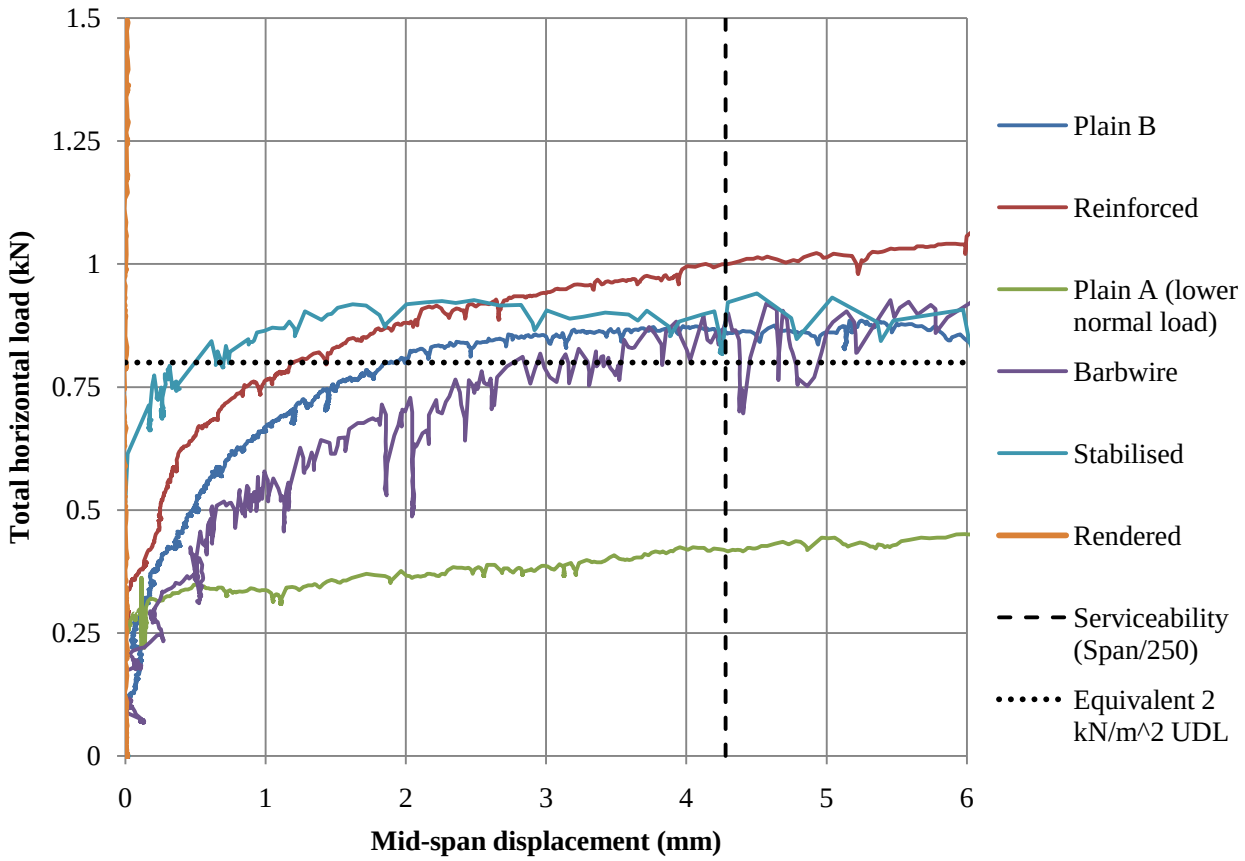

Figure 26 Horizontal load vs. mid-span displacement for flexural tests enlarged

Interestingly, 'Plain B' failed through two slip planes developing, with the second forming on the first interface below the bottom horizontal jack. Sliding continued until the second bag met the support, thereafter the wall began bending instead of sliding. Due to greater normal load, the increased frictional resistance of the interface between bag 2 and 3 became greater than the bending resistance of the wall. This transition took place when the total horizontal load exceeded 0.5kN, as evidenced by Figure 28 – this is part of a series of figures that map the transducer displacements and total horizontal load beginning on page 34.

Upon unloading, the majority of the displacements recorded by the transducers remained, since they were due to sliding failure. However there was notable recovery from displacements undergone during bending.

5.2.2 'Barbwire' model behaviour

The barbwire model behaved quite differently compared to the plain models. The added friction along the bag-to-bag interfaces led to a bending failure, as shown by the curved nature of the displacement plot in Figure 29. Higher displacements were seen for this model, in contrast to those of the 'plain' model, which indicated bending stiffness to be lower than the shear stiffness. When the load was released the curved shape was retained and the wall rotated away from the top support. This indicated that the bags' cross-sectional shape was altered from rectangular towards wedge shape with both permanent (plastic) and elastic (recoverable) alterations taking place.

5.2.3 Reinforced model behaviour

As with the 'barbwire' model, the reinforced model failed through bending. It is apparent from Figure 30 that the model's strength development had two phases. The first of which was elastic since it was recovered and repeated during an unloading and reloading cycle. Above this load the bags change shape permanently and the wall is less stiff globally. Peak strength was not reached.

5.2.4 Stabilised model behaviour

The first thing to note about the stabilised model performance was its similar strength (within 5%) to the non-stabilised model ('plain'). Furthermore both walls failed through sliding, yet the stabilised wall displayed significantly more shear stiffness. The displacement recovery after unloading was negligible (as expected) and the fill material remained hard intact blocks.

5.2.5 Rendered model behaviour

The render undoubtedly made a substantial contribution to strength and stiff. Approximately 5.5kN was the peak load applied before tensile cracking began, by which time only 5mm of deflection had occurred. The tensile crack appeared on the back face, level with the centre of bag no. 5, which as discussed is the section where the render is thinner than average. Compression cracking also appeared on the front face, directly adjacent to the loading plates.

Figure 27 Tensile crack (left) and compression cracking (right)

Once cracked, the render on the back face acted as two semi-independent plates with a hinge in the middle. The additional 2.3kN of strength achieved after cracking was due to the chicken wire mesh strain hardening as the strands became taught. Portions of the mesh pulled out of the render until they found enough resistance to begin straining.

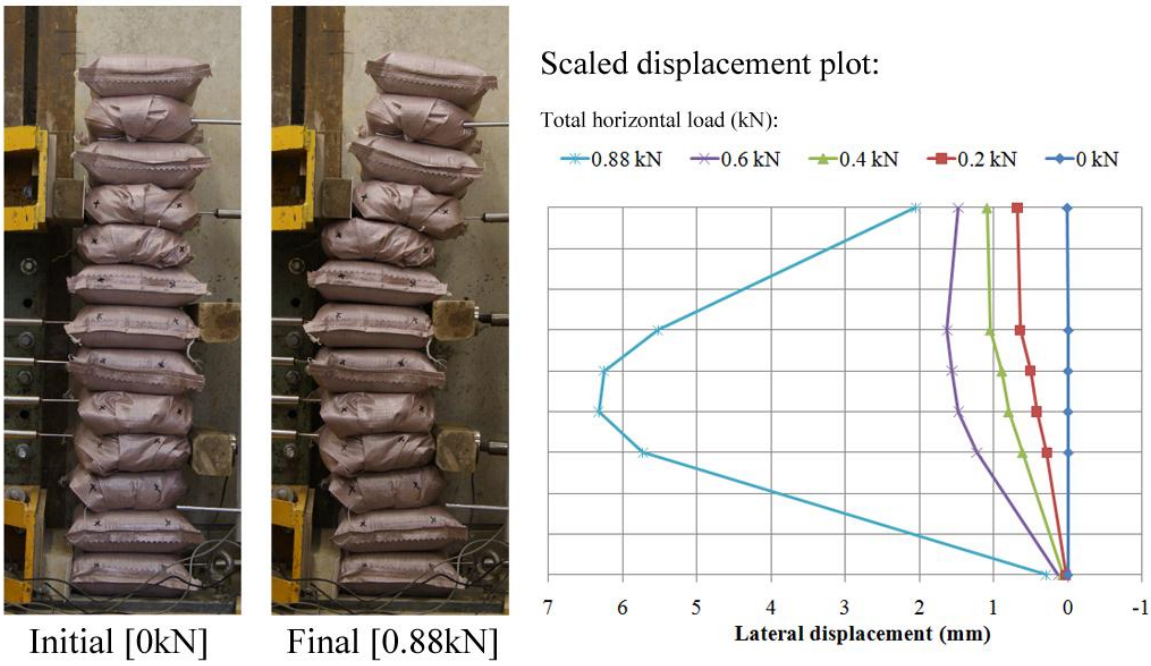

Figure 28 'Plain B': Initial and final state (left) lateral displacement vs. horizontal load plot (right)

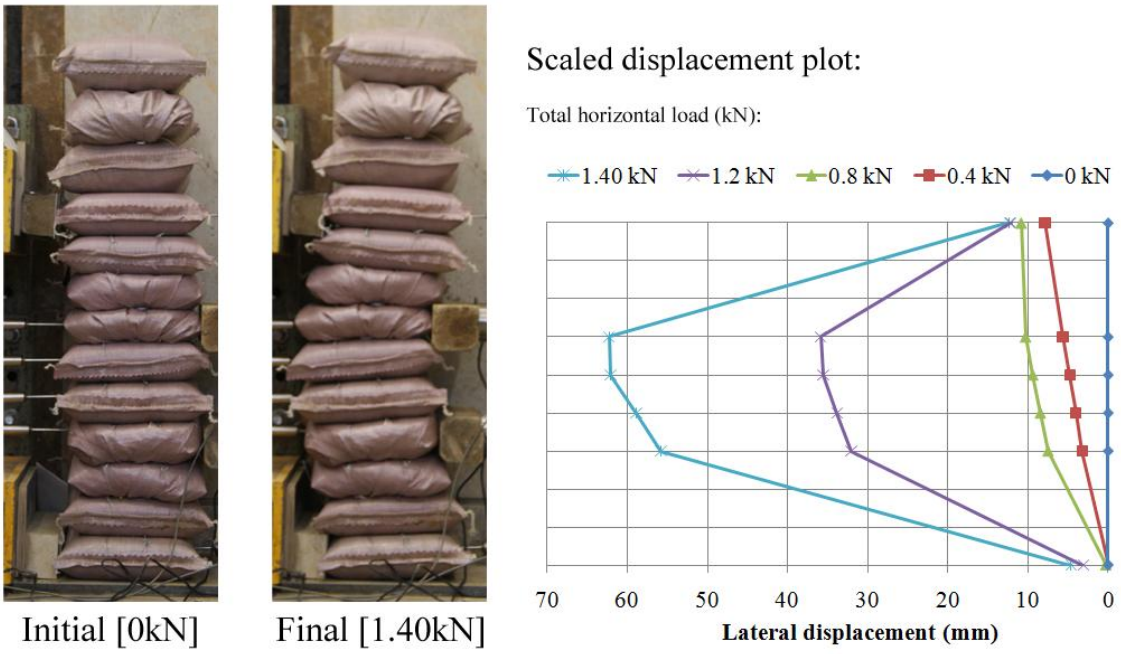

Figure 29 'Barbwire': Initial and final state (left) lateral displacement vs. horizontal load plot (right)

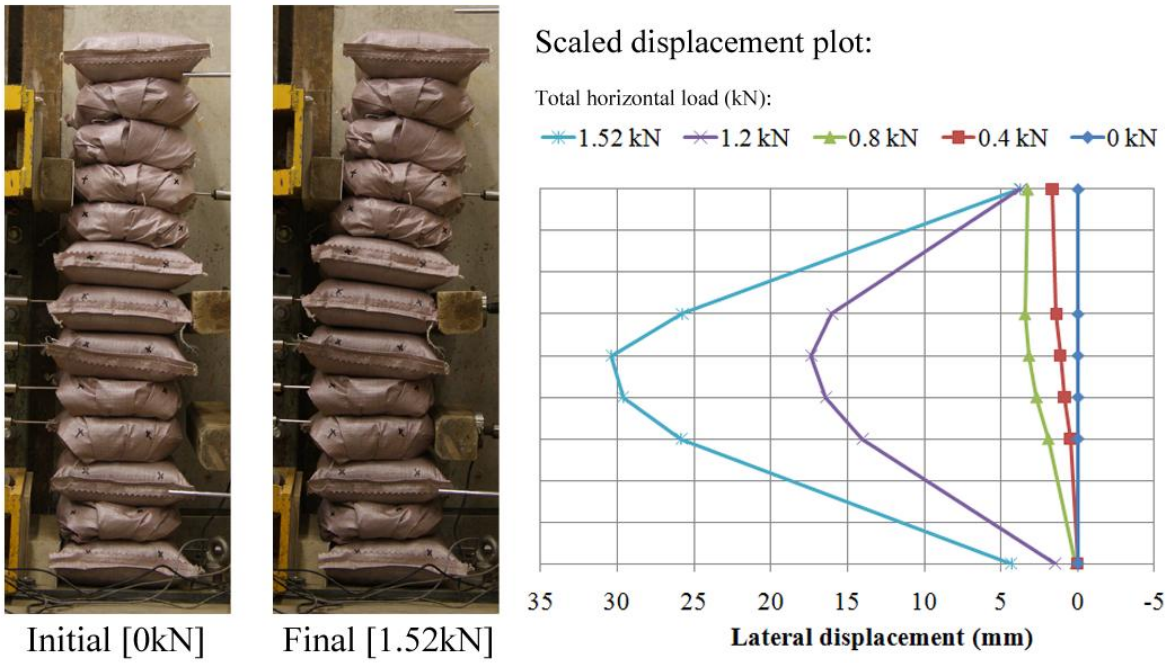

Figure 30 Reinforced: Initial and final state (left) lateral displacement vs. horizontal load plot (right)

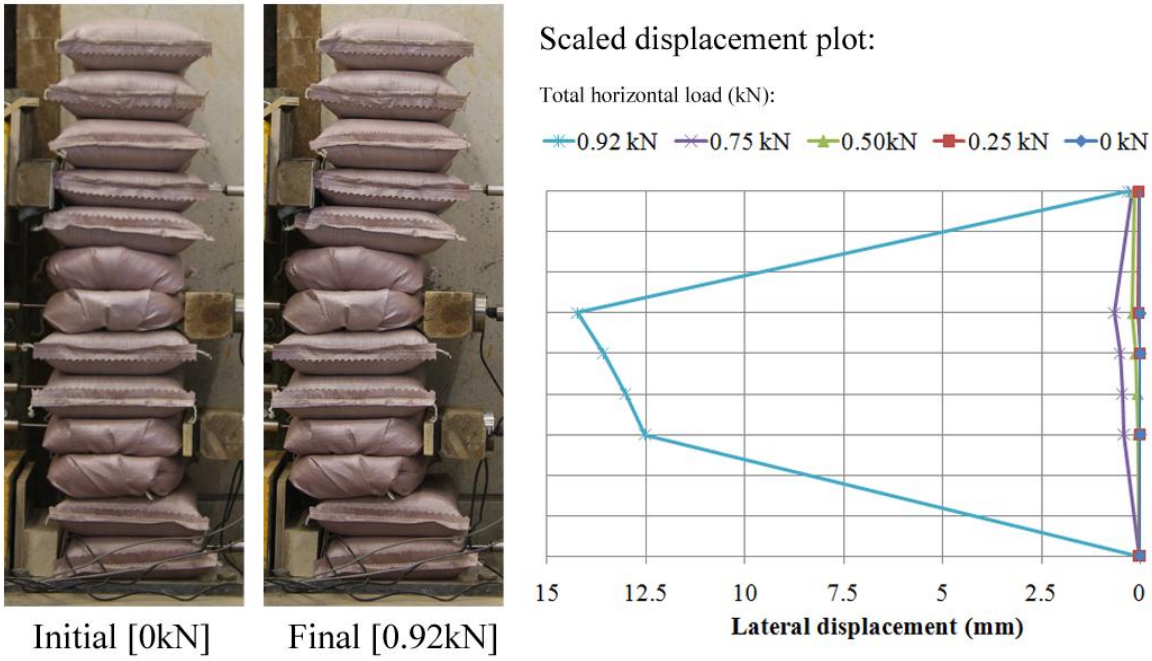

Figure 31 Stabilised: Initial and final state (left) lateral displacement vs. horizontal load plot (right)

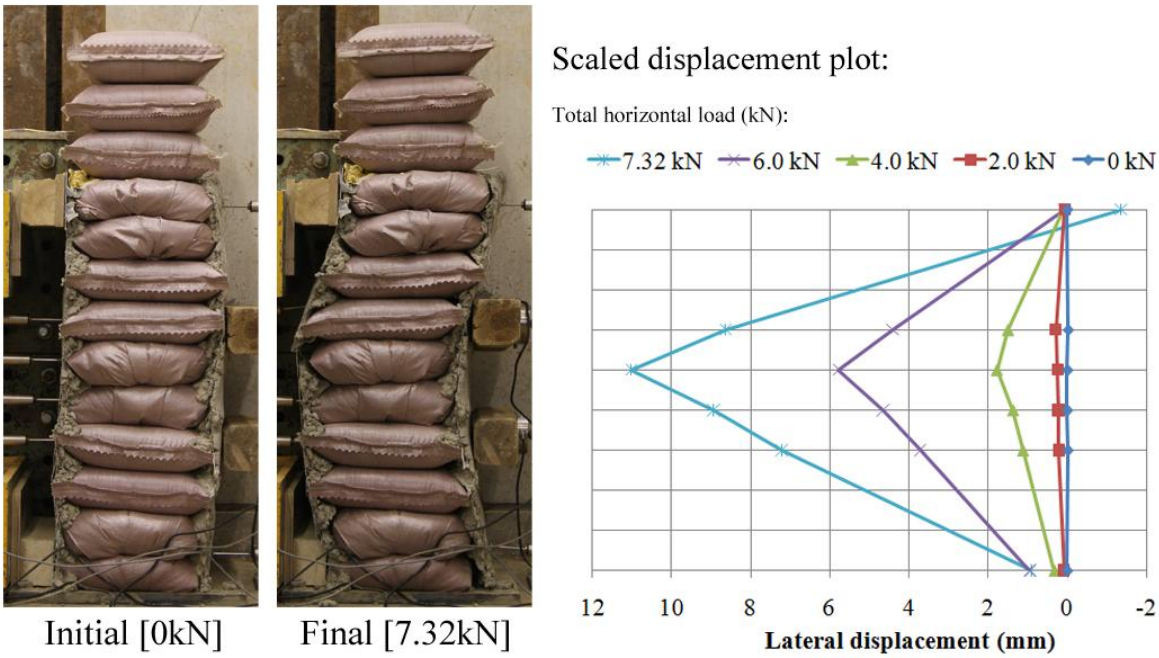

Figure 32 Rendered: Initial and final state (left) lateral displacement vs. horizontal load plot (right)

5.3 Analysis of flexural behaviour

5.3.1 Accuracy of predictions

For all models other than the reinforced model it is possible to compare the peak strength to a theoretical load. In the case of the reinforced model the highest loads achieved have been compared to the predicted failure load. Table 6 displays the both the achieved loads and predicted failure loads which have been calculated from results of material tests.

Table 6 Comparison between theoretical and experimental strengths of flexural walls

Wall model	Predicted failure load (kN)	Actual failure load (kN)	Accuracy model (%)
Plain A	0.169	0.46	$36.7^{(u)}$
Plain B	0.470	0.88	$53.4^{(u)}$
Barbwire	0.470	1.40	$33.6^{(u)}$
Reinforced	0.780	$1.52^{(1)}$	$51.3^{(u)}$
Stabilised	0.470	0.92	$51.1^{(u)}$
Rendered	22.9	7.32	$32.0^{(o)}$

Where: $^{(u)}$ *= Underestimate,* $^{(o)}$ *= Overestimate* $^{(1)}$ *= Highest load reached, not failure load*

It can be seen that the estimated strengths in each case were far from those seen in the experiments. There are many possible causes for inaccuracies in both the theoretical models and the experimental results. For each test they need to be clarified discussed.

5.3.1.1 Plain

The ‘Plain B’ model was predicted to fail through bending but it failed through sliding. This is deemed to the mainly to be the consequence of incorrect assumptions about the deflected shape and therefore strength of the theoretical model. By re-examining Figure 13 on page 14

then it can be seen that for the predicted deflected shape to occur (on the right) then free rotation of the bottom 'pinned' support is necessary. This was not the case in the experiment hence there was more resisting forces in the experiment than the model. Finally the contact area is a significant factor in the theoretical prediction and this was difficult to measure correctly after tamping had occurred.

Notwithstanding this, the actual failure mode of sliding can also be compared to the sliding model. Again, the experimental strength was greater than predicted which is a result of two slip planes developing rather than one. This may be explained by the same reasons above; that the deflected shape of a flexural wall with a single failure plane would require rotation at the base.

By redefining the theoretical model to incorporate two slip planes (with the second occurring below the bottom load) then the experiment can be further analysed. The modified sliding model over-predicts the shear strength, suggesting that either the interfaces were inclined or uneven in favour of the right to left translation seen. Alternatively Vadgama's (2010) value for the coefficient of friction between bags was higher than that of the bags used in this experiment.

Finally the model's physical conditions in general were not perfectly replicated by the experiments. The discrepancies affected all models and so have been left until the summary below in §5.3.2.

5.3.1.2 Barbwire

The results of the 'barbwire' test are very useful since the prevailing failure type was bending and therefore the result gives an indication of the actual bending failure strength of the plain model as well. The theoretical strength prediction was equal to the 'plain' model and indicated a force of 0.47kN was required to flex the wall, yet a force of 1.40kN was needed in practice. This result indicates that the additional restraint at the supports (and other discrepancies in the model) and possibly an underestimated contact area led to an underestimate of strength by a factor of three.

A further conclusion from the barbwire model is that the barbwire provides at least enough additional friction to act as a shear link between bags in a 1m high wall for this normal load. Therefore it will act as a shear link for greater normal loads higher too, as with increasing normal loads, the shear resistance increases at a higher rate than the bending resistance. This is illustrated for a 1m high 'plain' wall in Figure 15 (pg 15).

5.3.1.3 Reinforcement

The reinforced wall displayed varying stiffness at different stages as it was loaded. In the first stage it showed a higher stiffness similar to that of the barbwire model and in the second stage its stiffness decreased. This seems to indicate separate bending behaviour between the bags and the rebar. The theory that supposes the steel reinforcement is the sole provider of bending resistance above the bending strength of the bags alone. However, by calculating the applied moment on the steel due to additional loading then it was found that the steel should have yielded in the tests which it did not.

What actually happened is that a 'composite beam' formed where the steel reinforcement undertook the role of flange in tension and the half of the earthbags nearest the jacks (top of the 'beam') became the compression flange. This composite beam is stronger than the rebar

alone yet less stiff than an equivalent steel beam because of a lower effective Young's modulus. This explains the greater deflections seen by the reinforced model.

5.3.1.4 Stabilised

The stabilised model repeated the failure seen in 'Plain B' at a very similar load, that is, higher than the predicted loads which can be explained by the same reasoning above. The greater stiffness is a result of 'hard' fill which is stronger than the non-stabilised fill and therefore less susceptible to local deformations. This led to a higher stiffness.

The difference between a stabilised wall and a wall in bending is of interest because larger deformations/changes in geometry are needed for 'plain' walls to form deflected shapes. It is expected that, as with the arches tested by Pelly (2010) and Vadgama (2010), the harder fill will lead to a higher global strength.

5.3.1.5 Rendered

Unlike the theoretical models for the other walls, the model for the rendered wall overestimated the strength (and by a large margin). This could be due to lower render strength or lower render thickness in the experiment than compared with that used in the prediction. A further possibility is that the earthbags within the rendered faces are of different compaction and as such of varying stiffness. This could lead to uneven transfer of load from the face in contact with the loads to that being supported.

5.3.2 Conclusion

Each variable used in the test walls showed highly distinctive performance and behaviour from one another. The test setup influenced the possible failure modes due to physical infringements on the deflected shapes assumed by the theoretical model. Barbwire proved to be a sufficient shear link to prevent sliding failure, as did steel reinforcement, both leading to higher achievable strengths. In terms of performance the cement render clearly had the greatest impact; increasing strength of the plain model by over 8 times and the stiffness by 17 times.

Beyond the linear elastic limit the reinforced wall gained strength and residual strength was supplied to the rendered wall by the chicken wire. These are certainly beneficial characteristics for these variables. Overall the walls could withstand high deflections and maintained a high percentage of peak strength up to very large deflections (up to span/20 for the barbwire model). Finally, all walls resisted an equivalent loading of $2kN/m^2$ and most had reached peak strength at the serviceability deflection limit of span/250.

A summary of the potential errors in the theoretical models, the assumptions and the experimental results is given so further research can avoid repeating mistakes:

- Incorrect assumption of where yielding occurs and hence the actual failure load.
- Incorrect assumption of bag geometry incl. contact area and regularity.
- Support conditions – walls not purely simply supported and friction occurs between wall and loading plates.
- High variation in render thickness, strength and connection to bags and chicken wire, so a sample size of one is insufficient to gain a true representation.

5.4 Shear test results

Six shear tests were carried out as outlined in §4.2.2. In each test a fixed vertical load was applied initially. However, as the horizontal load increased the walls began deforming, the applied vertical load diverged from its original value. As stated above, the vertical stress has an influence on the frictional resistance and therefore with a varying vertical force the shear strength also varies. With this in mind, there is no single means of conveying the behaviour comprehensively. Instead several plots and figures are used to present the findings and allow analysis to be carried out.

One gauge for finding the strength of a wall is to identify the maximum ratio of horizontal load to vertical load (see Figure 33). In this set of experiments the rendered wall exhibited greater strength than the others, since it reached a higher ratio before failing. According, the plain model was the weakest with the lowest ratio reach upon failure. The tests are described in more detail below and plots of H/N vs. top course displacement along with the results from photogrammetry are displayed on pages - 44. Please note that in the case of the plain wall the relationship between H/N and displacement has been adjusted to include self weight in the normal load since the slip plane was known.

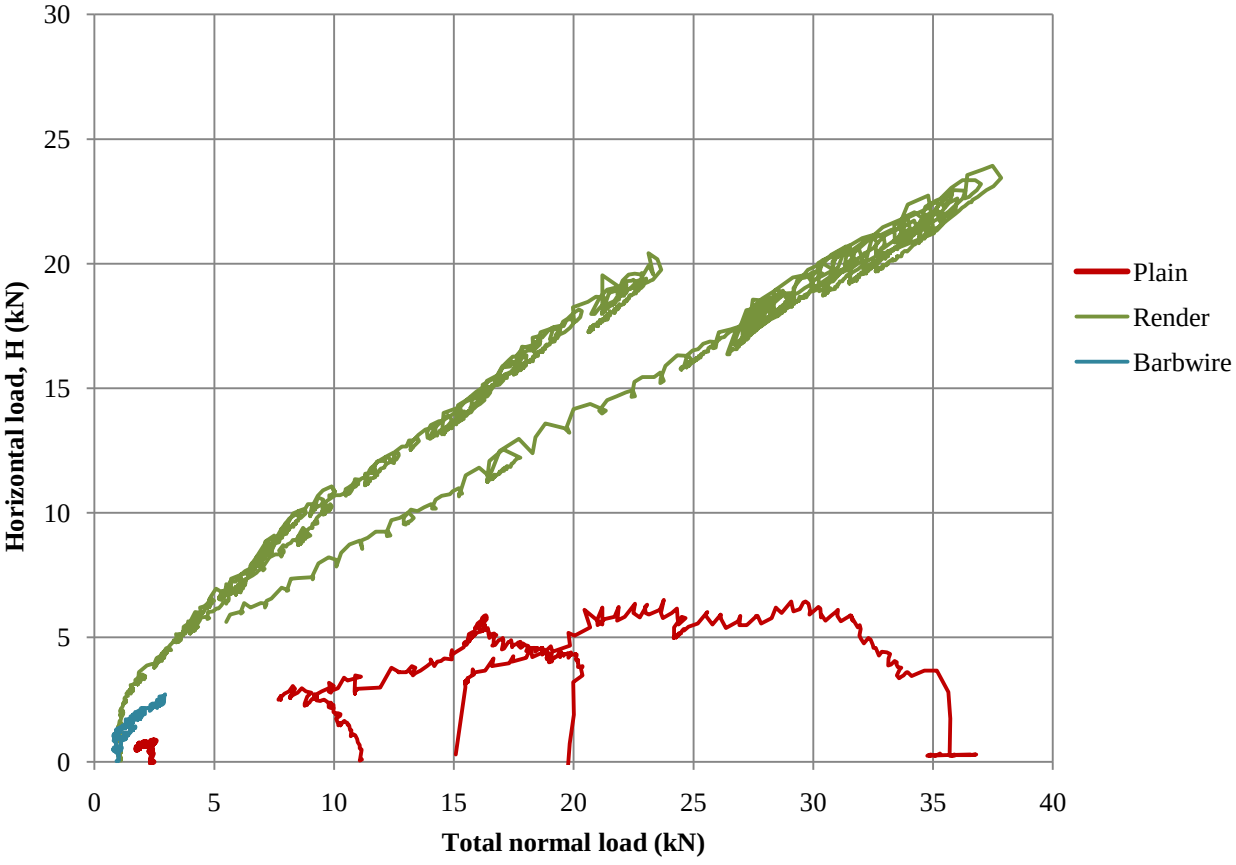

Figure 33 Horizontal load vs. normal load for all shear tests

5.4.1 'Plain' model behaviour

Three separate loading cycles were applied to the 'plain' shear wall which produced two different failure mechanisms. In the first load cycle the initial vertical loading totalled 1.0kN, yet this decreased as the shear load was incrementally added. The decline in normal stresses

continued until a diagonal bed joint slip plane developed when the ratio of horizontal load to normal load reached 0.36. The translating partition moved downwards as well as sideways, which relieved the normal stress given by the fixed displacement.

The downwards movement was the consequence of two changes in the wall. Firstly, the shear forces increased the normal forces on the far end of the wall which in turn compressed the bags more towards that end. Secondly, the ends of the wall consisted of half bags which were more difficult to confine as there was more bag material to tie under the bags when tamping. This led to even greater compaction occurring at the far end, which created a negative slope for the slip plane and therefore one of less resistance.

If we examine the plot of H/N vs. top bag displacement in Figure 37 then we can observe that beyond the H/N ratio of 0.36 the ratio eventually continues to increase. This is misleading because in reality, since the compaction had occurred more on the right hand side, the right hand normal load was less than that of left. Therefore the normal stress had reduced along much of the slip plane, yet the average remained higher.

For the subsequent load cycles higher normal loads were applied which also led to sliding failure. Both the uneven loading and the sloping bed joint phenomena explained above transpired for these tests. This amplified the distortion in the results in an incremental manner, correlating to increases in normal load. Thus the cycle with the greatest applied normal load (which averaged 23.7kN) had the lowest peak H/N ratio of 0.32. As can be observed in Figure 37, greater lateral displacement is experienced before peak strength and this corresponds with the lateral expansion under increased normal load.

Interestingly, the majority of the compaction was elastic (as evidenced by the displacement recovery), which indicates that the bag material was elongating to allow the bags to expand laterally to accommodate shortening.

Figure 34 Initial shape (left) and final shape (right) for 'plain' model test cycle 4

5.4.2 'Barbwire' model behaviour

Two loading cycles were carried out on the barbwire model, neither of which produced failure through sliding. Even during large displacements the frictional resistance was sufficient to

transfer shear stresses across the wall. The shear force led to a compression failure similar to that of the plain model with higher normal loads. In fact because of this increased bonding, the wall rotated about the centre of the base as well as compressing, which can be seen from photogrammetry output in Figure 39.

A peak ratio of horizontal load to normal load of 1.44 was reached for the second cycle. However, this ratio occurred at a displacement of 27.8mm. At this point there was an imbalance in the applied loads, hence this is an incorrect indication of strength. Furthermore, because sliding failure had not occurred at this peak, it was seen as unnecessary to conduct further experiments with higher normal loads since they would replicate the result.

5.4.3 Rendered

The circumstance for testing the rendered wall was different to the previous two walls, since the wall had enough tensile strength to rotate about the base. The top courses were compressed up to the render infill (Figure 35), which resisted bag movement. Subsequently the characteristic stepping down slip path of the 'plain' model could not develop. Additionally, by virtue of the wall lifting from the floor, there was a great moment on the rebar, which duly bent within the wall between the timber and the top course of bags.

The loading was increased in cycles and large rotations occurred for each cycle. In the final cycle a 35kN normal load was initially applied. Rotation caused the angle between the jacks and wall to alter. The increased normal load was transferred through the compressed bags until it finally cracked the render when the angle was such that only a short length of render was below the right-hand jack (see Figure 41).

The DEMEC readings show that compression took place in all directions in the centre of the render (on both sides). This compression proved very small compared to the compressive strength with the maximum compressive stress being 5.65% of the strength and the average only 3.68%.

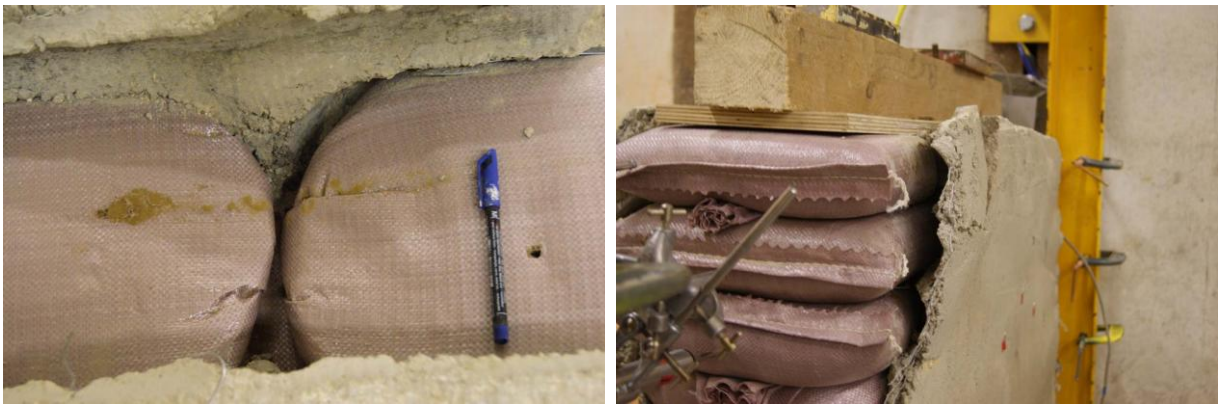

Figure 35 Compression of bags up to render infill (left) and separation of bags from render (right)

Figure 36 Result of photogrammetric analysis for 'plain' with average total normal load of 0.85kN (cycle 1 on graph below)

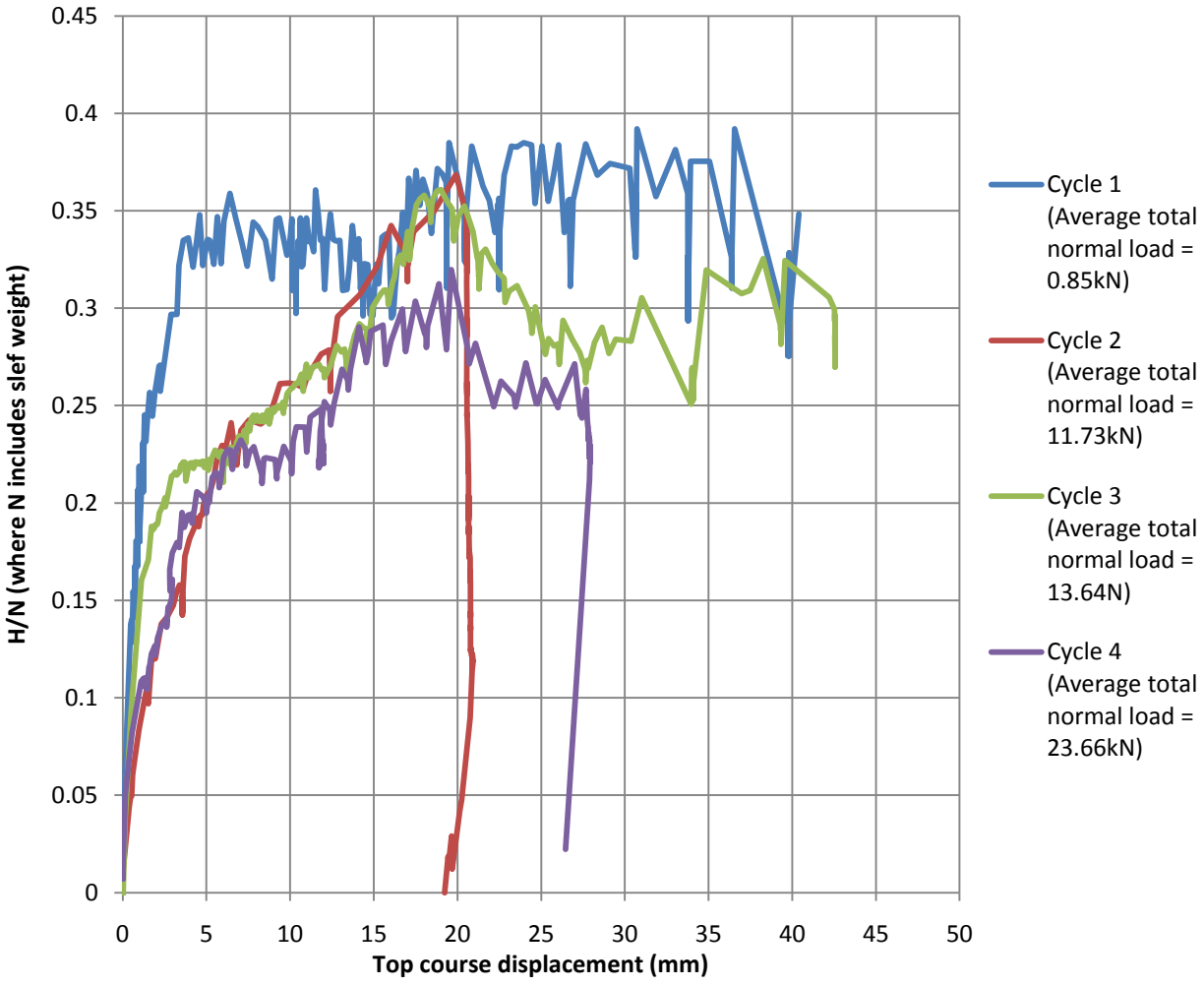

Figure 37 H/N vs. top course displacement for 'plain' wall (incl. self weight)

Figure 39 Result of photogrammetric analysis for 'barbwire' with average total normal load of 1.44kN (cycle 1 on graph below)

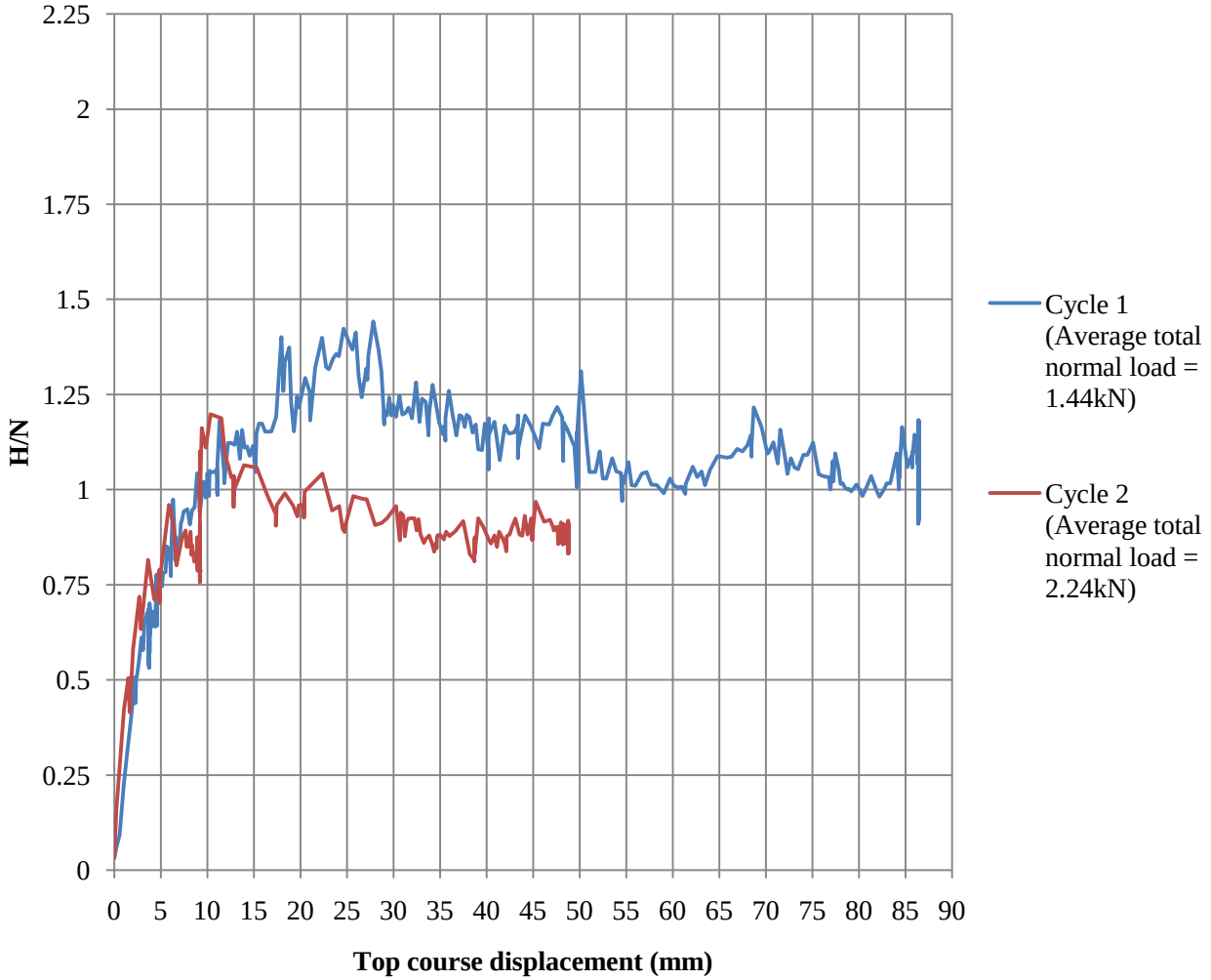

Figure 38 H/N vs. top course displacement for 'barbwire' wall

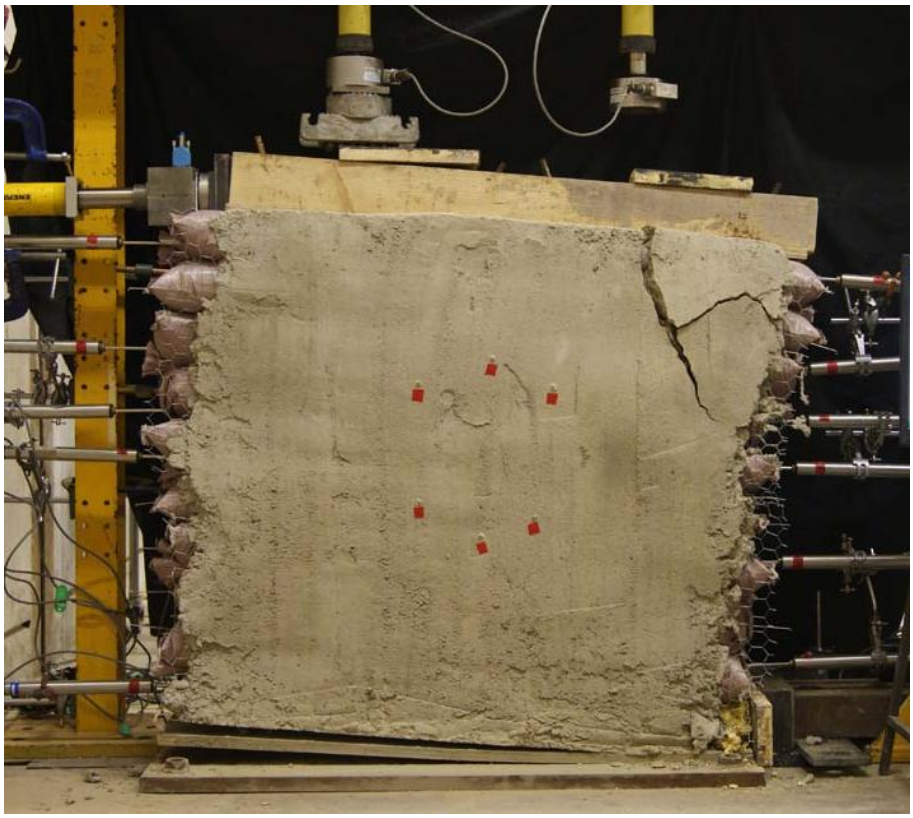

Figure 41 Final image of rendered wall at failure

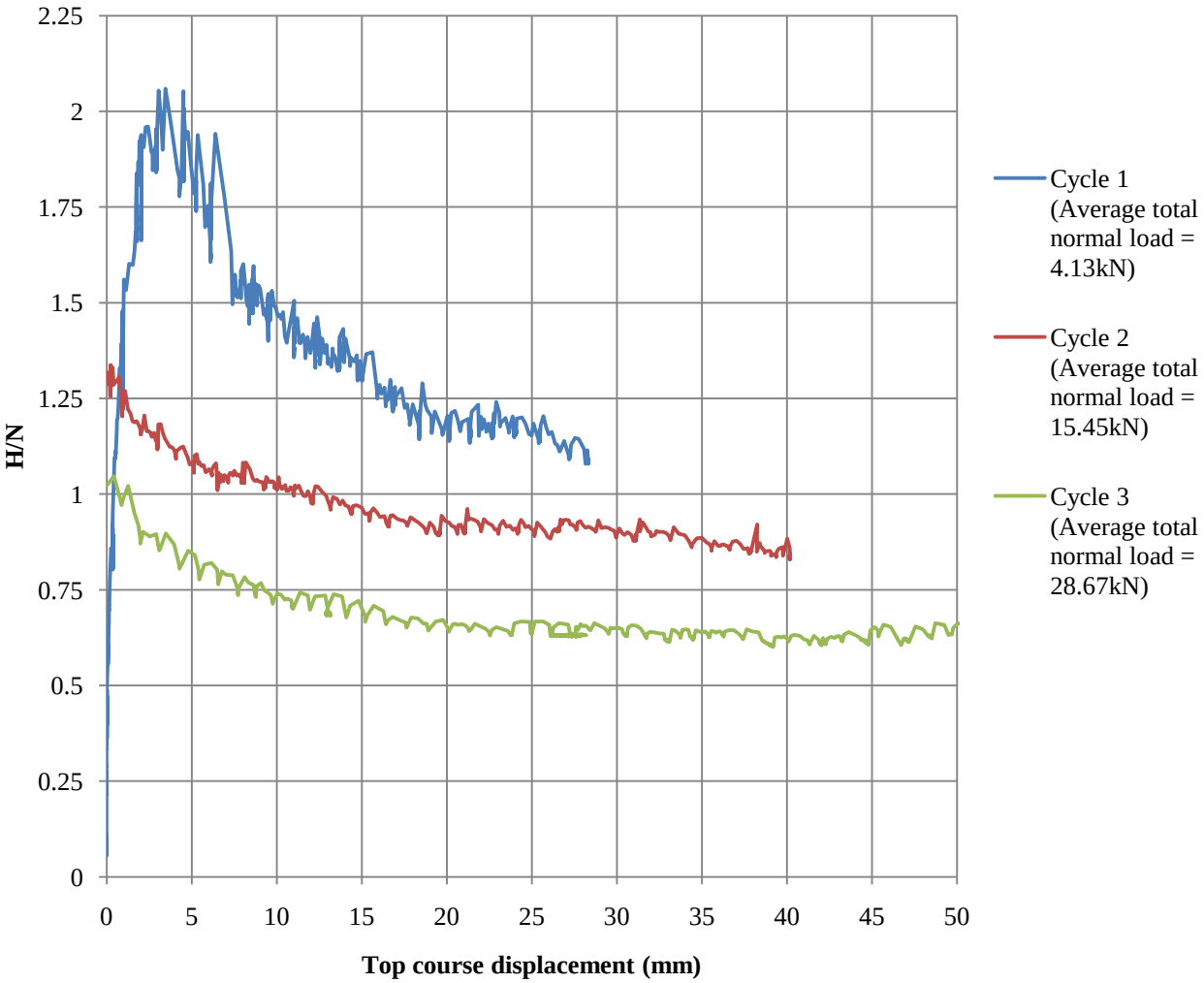

Figure 40 H/N vs. top course displacement for 'rendered' wall

5.5 Analysis of shear behaviour

5.5.1 Accuracy of predictions

Unfortunately a direct comparison between the 'barbwire' and the rendered models and their accompanying theoretical models cannot be made, since neither failed in the criteria set out for the shear wall models. This was due to compaction of bags for the 'barbwire' model and the rotations of the rendered model. Nonetheless the behaviour exhibited is very informative and allows significant conclusions to be drawn in this analysis. The strength exhibited by the plain wall, although it was subject to the same shape alterations, can be compared to the theoretical model, since a clear sliding failure occurred.

Table 7 Comparison between theoretical and experimental strengths of 'plain' walls

Wall model	Predicted failure load (kN)	Actual failure load (kN)	Accuracy (%)
Plain (N = 0.85kN)	0.81	0.77	94.2 $^{(o)}$
Plain (N = 11.7kN)	4.73	4.72	99.7 $^{(o)}$
Plain (N = 13.6kN)	5.42	5.25	97.0 $^{(o)}$
Plain (N = 23.7kN)	9.06	7.53	83.1 $^{(o)}$

Where: $^{(u)}$ *= Underestimate and* $^{(o)}$ *= Overestimate*

5.5.1.1 Plain

As Mann and Muller (1982) correctly theorised for masonry, the alternative stepped sliding pattern also occurred for the plain earthbag shear wall. The theory showed a very close correlation with the reality, with up to 99.7% accuracy and a minimum of 83.1%. In each case the predictions overestimated the strength. This is thought to be a result of the compression of the right-hand portion of the wall, creating a sloping and thus less resistant path.

The failure envelope suggests that compressive failure of bags will not occur until very large normal loads are experienced (see Figure 18, pg 21) and in the experiments carried out compressive failure did not occur. However, there was a large amount of vertical compaction and the resulting deformation could be considered to equate to a serviceability failure.

5.5.1.2 Barbwire

The same deformation occurred for the 'barbwire' model, which can be considered a serviceability failure. The top course of the wall displaced over 100mm in each load cycle and Figure 38 (pg 43) suggests 77% of its peak strength was maintained at these displacements. In reality a higher proportion was maintained because the H/N ratio distorted at large displacements.

During the 'barbwire' model test a low global stiffness of the wall in compression was also apparent. Unfortunately since this is thought to be due to the less confined half bags compressing, it is not valid to make any comments regarding likely vertical stiffness of earthbag structures.

5.5.1.3 Rendered

The rendered wall was subject to very high normal and shear loads before cracking. It is incorrect to take these values as the strength, because although the friction between bags obeyed the Mohr-Coulomb condition the render did not. The normal stresses served to counteract tensile stress in the render. However, once either the tensile/shear/compressive strength of the render is exceeded, which is possible under relatively low loads, a local

premature failure may occur. Consequently the conditions in which the rendered wall is loaded (i.e. roof connections and bearing conditions) are very important.

The recordings of H/N vs. top course displacement in Figure 40 would suggest that a higher ratio of H/N is achievable for lower normal loads. In fact, at lower normal loads the wall was less compressed initially and upon rotation this allowed the wall to compress under the left hand vertical jack which in turn allowed both jacks to apply larger normal loads.

Although the wall did not fail globally, individual elements such as the render and rebar bending failed locally. Render stresses from DEMEC showed that stresses were not critical in the centre of the wall; yet it failed through cracking in the top right. Therefore the render's distribution of stress contradicts the assumed crack path given in Figure 21. It is unknown whether this crack path would occur for walls that do not rotate, since the whole state of stress within the wall was altered.

As mentioned above, the steel reinforcement that was inserted through the timber beam into the top three courses was bent (to varying degrees). Once the wall had rotated it was the reinforcement that held the rigid wall to the underside of the beam. It can be said, that in a similar vein for the cracking of the render, the rebar bending was due to the rotation of the wall in this particular test and therefore is not a universally applicable result. Conversely, if rotation was prohibited it is likely that bending of the rebar would still take place. In Figure 42 the rebar have been set out in order of how they were located in the wall. (It should be noted each bar was facing the opposing direction in the wall, i.e. the left-most rebar bent clockwise.)

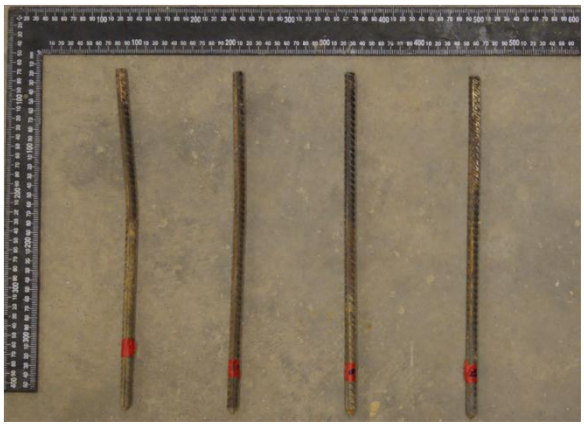

Figure 42 The steel reinforcement used in the rendered shear wall (shown in order)

Upon discovering the rebar bent before the render cracking, the question arises as to whether a failure mechanism involving rebar bending is more critical than that of shearing of the render. If the rebar is assumed to be vertical and fixed in bags and that it is the sole connection between the timber beam and the bags (i.e. the nails between the timber plate and the bags are ignored) then the horizontal loading capacity can be investigated. If the rebar is loaded by the centre of the beam and all 4 bars are loaded simultaneously, then bending theory suggests that a maximum of 4.0kN can be applied horizontally to the timber beam.

How does this compare to a theoretical global failure through the render? If we also consider a rendered wall where rotation is prevented, the assumed global failure is a crack along the stepped failure surface of the plain wall as shown in Figure 21. If the crack is formed purely through tension (which is weaker than the shear strength) then a failure load of 455kN is

found. This is over 110x the force needed to bend the reinforcement, so although these are very approximate calculations, it can be said that in this system it is global failure is more likely to occur by the timber rafters bending the reinforcement than the render shearing.

5.5.2 Conclusion

It is clear from the results that both rendering the wall and laying barbwire between courses, causes significant improvement in strength. A global failure was seen for the 'plain' model and provided a reference from which to assess the further two models. However, these models showed sufficient strength that the nature of the testing hindered the investigation to define their capacity.

In all three tests the vertical loads were applied through fixed displacements which led to deviation from the initially intended normal load. This led to non-uniform compression in the walls because they compressed unevenly upon rotation and hence unsymmetrical loads were thus applied through the vertical jacks.

The rendered wall did display very high load carrying performance, but the testing but did not define its global strength. Instead the test highlighted potential local failures and indicated that failure between the timber roof and the top courses of bags was the limiting factor in the wall's strength.

The potential errors in the theoretical models, the assumptions and the experimental results for the shear wall are given here:

- A non-uniform vertical compression was inherent, due to applying fixed displacements, which led to modification of the wall geometry and stress distribution.
- Half size bags compacted more than the full size bags and altered the overall geometry.
- The limited length of the wall influenced the failure modes, including rotation.
- There was great potential for large variations in the build quality for all walls. Thus a sample size of one is insufficient to gain a true representation.

6 Discussion

A brief discussion on the validity of the experiments and theoretical model, as well as the potential implications of the results (for both the design and the assessment) for earthbag housing studies is set out in this chapter. Recommendations for future studies have also been made.

6.1 Validity of results

A direct comparison with corresponding tests made in preceding investigations cannot be made, since these are original tests. The methodology can be critically evaluated through inspection of the results and it is cannot be denied that both types of lateral strength testing carried out here can be improved upon.

The first inadequacy can be found in the overall design of the experiments. Small dimensions were adopted for the size of the wall, which allowed end restraint effects and premature failures to be incurred. Conversely, the effects of phenomena that only occur for full size walls, such as buckling, may have been overlooked. In addition, only one bag thick walls were examined, which neglects designs of two bags or more thickness. Therefore testing a range of lengths and thicknesses for full height walls would produce more representative results.

Fluctuation of the twin loads applied in the flexural test was seen due to the use of two separate hydraulic jacks. This was one of many discrepancies between the theoretical models and the laboratory tests. The most significant discrepancy was the variation in normal load for the shear test which made direct analysis less accurate. When this is combined with the fact that rotation and/or compression of the wall also imposed undesired normal loading then clearly the shear wall test can be improved.

A recommend alteration to the shear test is to hold down the edge of the wall that the lateral load is applied to. This step is often taken for racking tests for masonry walls and prevents rotation of the wall. The top loads could also be modified by using a computer controlled jacks that apply a constant normal load, or simply attaching a weight.

Finally, the testing only modelled very simple loading mechanisms, which may not impose the worst case loading. For example, the in-plane lateral loading was only applied through the roof, whereas seismic loading from the ground could be more critical. In the flexural wall test the effect of different normal loads on the flexural wall was not seen on models other than the ‘plain’ model.

6.2 Implications of experimental results

Despite the criticisms highlighted above, both the flexural and the shear strength tests indicated that the render is undoubtedly the largest contributor to strength in the Hunter and Kiffmeyer (2004) model. With the addition of barbwire and the reinforcement stakes, this design certainly has great strength and stiffness. Whether these additions are sufficient to meet building standards is up for questioning since large material safety factors are generally applied to highly variable building materials such as this.

Local failures are possible, especially if the connections to the roof and the adjacent walls create non-uniform load bearing or bearing directly onto render. For non-rendered walls only one bag wide, both the strength and the stiffness are insufficient. On the other hand their

capacity to withstand large displacements before ultimate failure is encouraging. Finally, if it is only extreme and rare loading conditions that cause bag movement then the deformable nature of the bags allows reposition or even re-building.

6.2.1 Implications for out-of -plane loading

For the walls tested in this investigation two strands of barbwire were sufficient to prevent sliding failure (with a small normal load) and stabilisation improves the stiffness. The wall height was only 1m and it was clear that the support conditions distorted the results. For greater heights the effect of the non-idealised support conditions would be reduced and therefore strength is likely to be estimated more effectively.

The capacity of an earthbag wall to sustain out-of-plane deformation is smaller than the same capacity in regards to the in-plane direction. When this characteristic is combined with the lower strength for this direction then sudden failure for walls in the-out-plane direction becomes the most critical ultimate failure mechanism.

6.2.2 Implications for in-plane loading

The strength of the wall in shear is to a great extent a function of the length. For earthbag walls to act as effective shear walls then a minimum length is therefore required. Furthermore, this length could also be subject to adjustment, depending on the walls stiffness, as it is probable that the serviceability limit state is critical.

If the walls are rendered then it is likely that the connection to the roof is critical for the strength, yet the system still has a high capacity. Therefore for non-rendered walls, the stiffness and strength are again a concern for plain walls, although the addition of barbwire limit delays global failure.

6.3 Recommended Future Studies

There have been few experiments in the field of earthbag building structures and there is certainly a cause for further work to been done. Although it is not only the unanswered structural engineering questions that require investigation, they will be the focus here, given the aims of this research. As pointed out above, there is cause for additional shear and flexural tests on earthbag walls. A further argument would be to test more fill types, bags types (including tubing) and render types to produce a greater body of research upon which theoretical models can be evaluated.

Earthbag structures often come in curved forms (such as domes) and a worthwhile investigation would be one that compares architectural form alongside strength. Curved wall forms entail different strength characteristics under lateral loading, not only because of effects such as hoop stress, but also due to geometrical differences for elements such as the render. Vernacular earthen architecture often adopts forms that perform well in compression since earthbag materials (including earthbags) perform badly in tension. This approach should be adhered to if efficient earthbag structures are to be designed.

Ultimately, the seismic resistance of earthbag houses is of great interest due to their presence in areas prone to seismic activity. Dynamic loading is certainly the most challenging to model because of difficulties in scaling forces and accelerations for smaller models. Their deformable nature would suggest that earthbags structures could dampen accelerations, although since they are massive, the natural frequency may pose a problem.

7 Conclusion

The performance of earthbag walls under horizontal loading has been investigated through the creation and development of theoretical models and by the testing of physical models. The theory behind the behaviour of earthbag walls, subject to both in-plane and out-of plane horizontal loading, was examined. Subsequently the models were presented which predict the linear elastic limit through the application of bending theory and a modified Mohr-Coulomb theory.

A flexural test wall design was modified to include variables such as placing barbwire between courses, steel reinforcement, stabilised bags and cement render (on both the front and faces). For the shear tests, a conventional walling system was by investigating the effects of rendering and laying barbwire between courses only.

The profound result was that the cement render increased flexural strength and the shear strength by a considerable margin. The flexural strength of the 'plain' model was raised by a factor of 7 (from 0.88kN to 7.32kN) and stiffness by a greater extent. Although a global strength could not be resolved for the shear wall test, the rendered wall proved stronger than the steel and timber roof connection which failed through the 10mm rebar bending.

The action of adding two strands of barbwire between courses also increased the strength in both planes. For the flexural strength barbwire improved the plain model strength by a factor of 1.6 although it displayed notably less stiffness. Of the remaining variables in the flexural tests, the steel added the second highest amount of strength. The 10mm bar sustained large deflections and consequently the peak strength was not achieved (max load = 1.52kN). Stabilisation of the bags was found to exhibit similar strength yet minimise deflections and therefore outperform the 'plain' model under serviceability criteria.

In the out-of-plane loading both bending and sliding failure was considered by the theoretical models. Laboratory tests differed from the model predictions in some instances by a factor of three. This was explained by imperfect modelling of the theoretical model. The support conditions, the variation in contact area of bags and uneven bed joints are cited as causes of the disparity.

Difficulties arose in keeping loading conditions constant for the in-plane loading and accuracy of the results was undermined by the compression of bags due to variation of normal load. However the modified Mohr-Coulomb approach, previously used for masonry walls, proved suitable in the assessment of plain earthbag shear walls.

This research has included a range of permutations and set a precedent for future analysis of earthbags under lateral loading. However, there are many more loading scenarios and material types to investigate, in order to broaden the field of knowledge of how these structures behave and allow further use of this low-cost and low carbon material.

Bibliography

Bosiljkov, V., Page, A., Bokan-Bosiljkov, V. and Žarnić, R. (2010), Evaluation of the seismic performance of brick masonry walls. Structural Control and Health Monitoring, 17: 100–118.

BS1377-2:1990. (n.d.). Methods of test for Soils for civil engineering purposes. *Part 2: Classification tests*. BSI.

BS EN 12390-3:2009. (n.d.). Testing hardened concrete. *Compressive strength of test specimens*. BSI.

BS EN 12390-5:2009. (n.d.). Testing hardened concrete. *Flexural strength of test specimens.* BSI.

Calderini, C., Cattari, S. and Lagomarsino, S. (2009), In-plane strength of unreinforced masonry piers. *Earthquake Engineering & Structural Dynamics*, 38: 243–26.

Daigle, B. (2008). Earthbag Housing: Structural Behaviour and Applicability in Developing Countries. Thesis (M.Sc.) Queen's University, Kingston, Ontario, Canada.

DeJong, J., & Frost, J. (2002). Physical evidence of shear banding at granular-continuum interfaces. *15th ASCE Engineering Mechanics Conference*, (pp. 1-7). Columbia University, New York, NY.

Dunbar, R. (2006). Prism Test of Earthbags. Undergraduate Research. West Point Military Academy.

Graubner, C-A. and Kranzler, T. In-Plane Bearing Capacity of Unreinforced Masonry Panels. *Proceedings of the 7th International Masonry Conference*, London, 2006

Hunter, K. and Kiffmeyer, D. (2004). *Earthbag building - The Tools, Tricks and Techniques.* Canada: New Society Publishers.

Khalili, N. and Vittore, P. (1998). Earth Architecture and Ceramics: The Sandbag/Superadobe/Superblock Construction System. International Conference of Building Officials, Cal-Earth Institute, Hesperia, CA, USA.

Lohani, T., Matsushima, K., Aqil, U., Mohri, Y., & Tatsuoka, F. (2006). Evaluating the strength and deformation characteristics of a soil bag pile from full-scale laboratory test. *Geosynthetics International*, 13 (6), 246-264.

Mann, W. and Müller, H. (1982). Failure of shear-stressed masonry - an enlarged theory, tests and application to shear walls. *Proceedings of the British Ceramic Society 1980*; 27:223–235. British Ceramic Res. Assoc.: London, England,

Matsuoka, H., & Liu, S. (2003). New earth reinforcement method by soilbags ("Donow"). *Soils and Foundations*, 43 (6), 173 -188.

Minke G. (2006). *Building with earth*. Basel: Birkhäuser.

Pelly, R. (2010). Plastic limit analysis of earthbag structures. Dissertation (M.Eng.). University of Bath, Department of Architecture and Civil Engineering.

du Pisanie, N. (2009). Community building - Sustainable, appropriate desert building for the Topnaar communities of the Kuiseb River. *11th international conference on non-conventional materials and technologies*,6-9 September 2009, Bath. Bath: University of Bath Press.

Tantono, S. (2007). The mechanical behavior of a soilbag under vertical compression. Graz University of Technology, Institute of Applied Mechanics.

Turnsěk, V. and Čačovič, F. (1971). Some experimental results on the strength of brick masonry walls. *Proceedings of the 2nd International Brick Masonry Conference*, Stoke-on-Trent. British Ceramic Res. Assoc.: London, England, 1971; 149–156.

Vadgama, N. (2010). A Material and Structural Analysis of Earthbag Housing. Dissertation (M.Eng.). University of Bath, Department of Architecture and Civil Engineering.

Xu, Y., Jian, H., Yanjun, D. and De-an, S. (2008). Earth reinforcement using soilbags. *Geotextiles and Geomembranes*, 26 (3), pp.279-289.

Appendix A

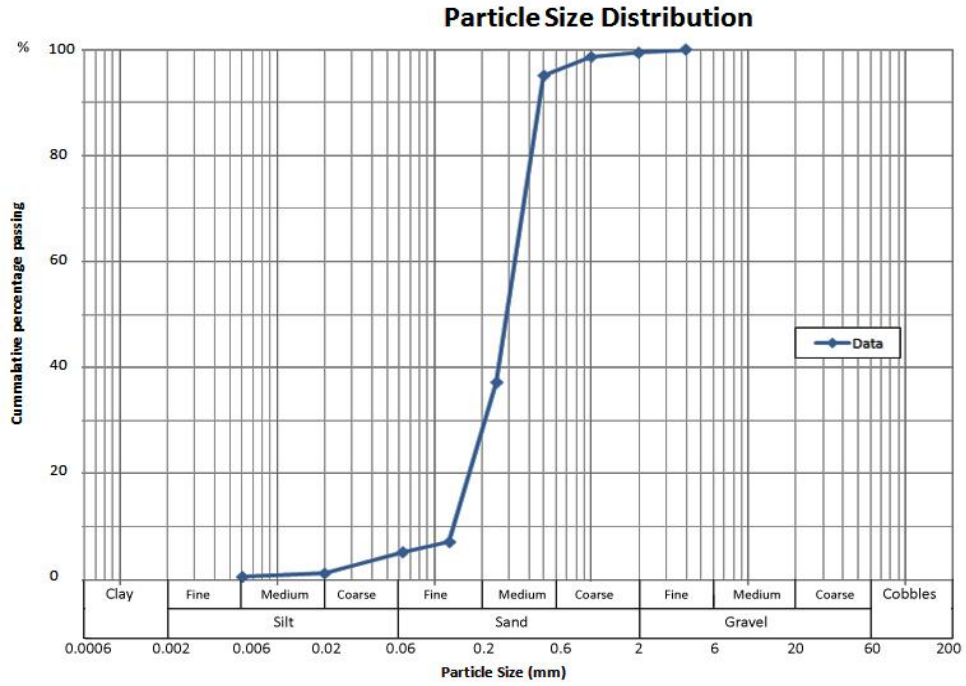

Figure 43 Dry sieve analysis of fill material

Appendix B

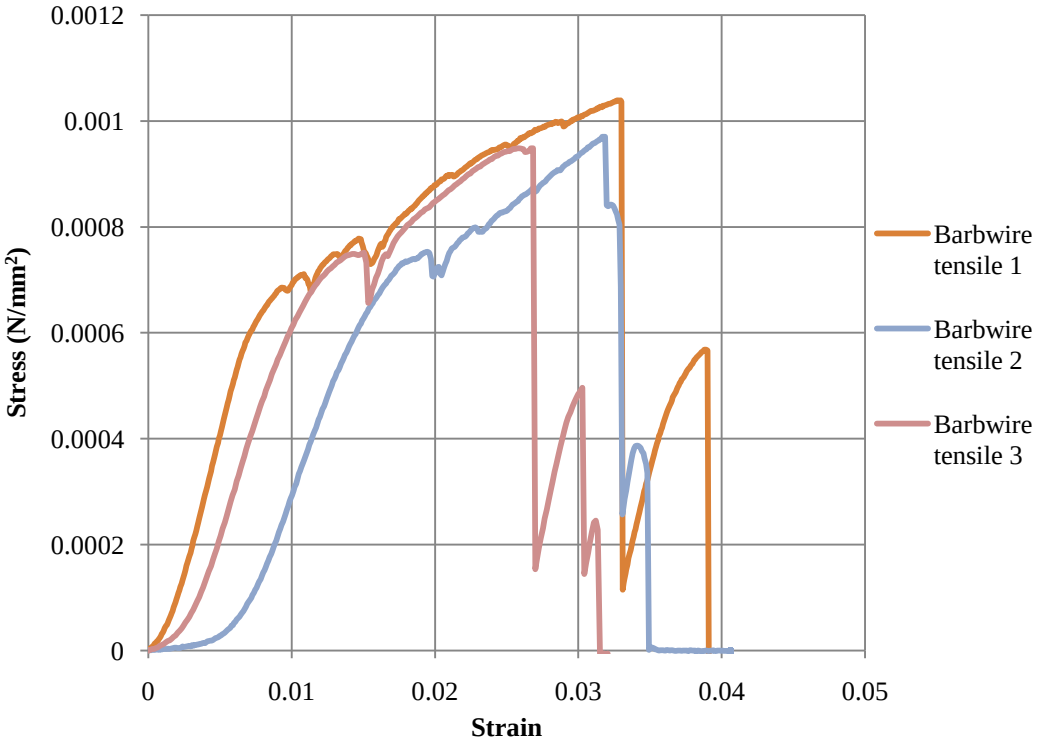

Figure 44 Stress vs. strain for barbwire tensile tests

Appendix C

Table 8 Render compression and flexural test results

Sample	Initial height (mm)	Initial width (mm)	Compressive strength (N)	Tensile strength (N/mm)	Young's Modulus (N/mm^2)
Render 1 (flexural wall)	40	40	10.02	3.45	681.8
Render 2 (flexural wall)	40	40	10.10	3.29	1830.7
Render 3 (flexural wall)	40	40	10.26	3.40	1995.1
Average (flexural wall)	-	-	10.13	3.38	1502.5
Render 1 (shear wall)	40	40	10.92	3.17	1509.1
Render 2 (shear wall)	40	40	10.98	3.28	2357.6
Render 3 (shear wall)	40	40	10.76	0.23	1751.4
Average (shear wall)	-	-	10.89	3.23	1872.7

Figure 45 Typical cross section of render prism used in flexural test

Appendix D

Table 9 Steel reinforcement axial tension test results

Sample	Diameter (mm)	Peak stress (N/mm^2)	Yield stress (N/mm^2)	Yield strain (%)	Young's modulus (N/mm^2)
1	10	660.6	556.4	0.236	198131
2	10	670.2	492.7	0.228	175137
3	10	668.1	486.4	0.229	182922
Average	-	666.3	511.8	0.231	185397

Appendix E

Table 10 DEMEC Stain gauge results

Group	Max strain (mm/mm)	Max stress (N/mm^2)*
1	-0.00031227	-0.58
2	-0.00018416	-0.34
3	-0.00031761	-0.59
4	-0.00032829	-0.61
5	-0.00005338	-0.10
6	-8.8077E-05	-0.16
Average	-0.00021396	-0.40

**Where: E = 1872.7N/mm^2 and $\sigma_{c,max}$ =10.89 N/mm^2 and (-) = compression*

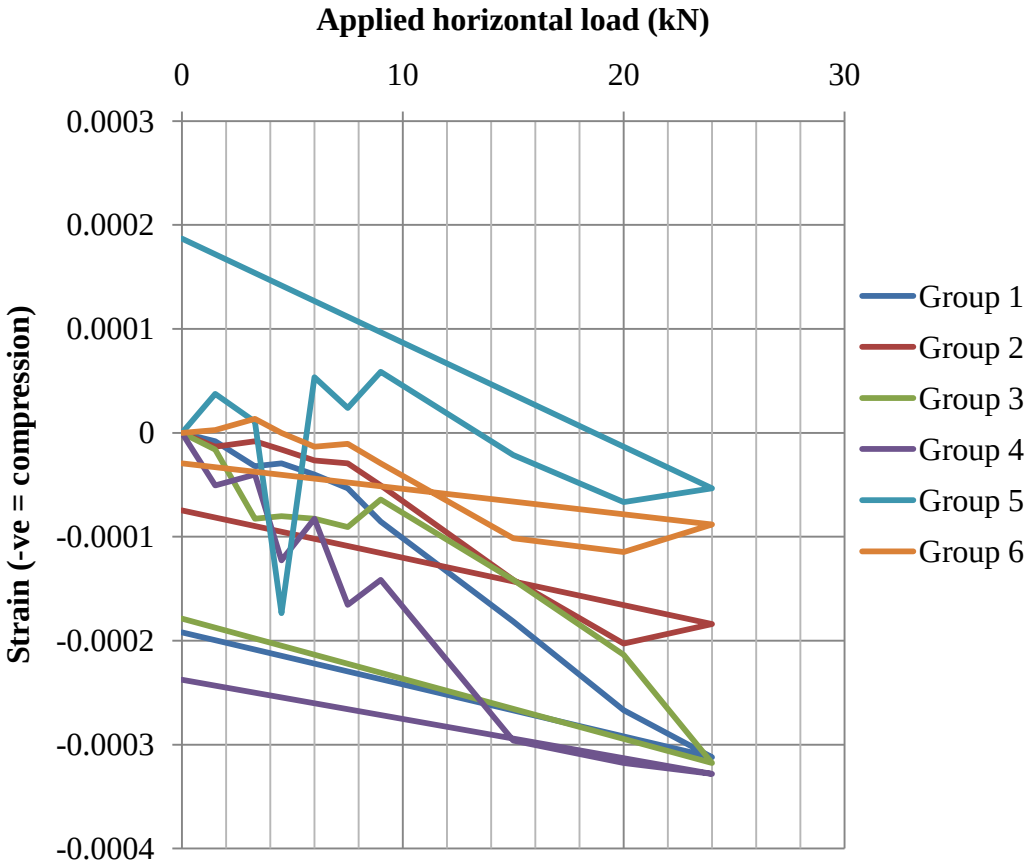

Figure 46 Applied load vs. strain for DEMEC marker groups